treatment.

The principal finding of our study was that baPWV progressively improved during long-term successful anti-hypertensive treatment with benidipine. The improvement was maintained following correction for BP changes, after 6 months of treatment (Fig. 2). Moreover, baPWV and BP remained at lower levels 2 weeks after suspension of benidipine (Table 1). These findings strongly suggest that the arterial properties of patients are improved by benidipine in conjunction with prolonged successful BP reduction. Benetos *et al.* (*20*) reported that PWV increases with age even in normotensive subjects and that the increase is greatly accelerated by co-existing high BP, high heart rate and high serum creatinine. Ichihara *et al.* (*10*) also reported significant reductions of baPWV following intensive BP lowering in a group of hypertensive patients, but not in a group undergoing moderate BP lowering. These findings, as well as those of the present study, highlight the importance of good control of BP for preventing or reversing the hypertension-induced progression of arterial stiffness.

Benidipine and nicardipine bear a close resemblance in the clinical setting; in a multi-center trial in Japan, the two drugs demonstrated comparable BP lowering capacity and minimal influence on pulse rate (*21*, *22*). Benidipine, however, seems to have a higher efficacy than nicardipine in coronary and glomerular arteries (*23*, *24*). In addition to BP lowering capacity, benidipine has beneficial effects on the vascular wall: benidipine improves endothelial function *via* stimulation of nitric oxide synthesis and inhibition of endothelin-1 expression (*16*, *18*, *25*). Benidipine also has an anti-oxidative action in hypertensive patients that could contribute to the prevention of arterial sclerosis (*26*). In addition, the ratio of baPWV reduction to BP lowering by benidipine in the present study was larger than those in previous reports (*10*, *11*). Thus, additional benefits of benidipine may include a contribution to the improvement of arterial properties, but further study is needed to confirm this. CRP is thought to be a predictive, causal and therapeutic marker of cardiovascular disease (*27*, *28*), and a decrease in CRP levels has been associated with good outcomes (*28*). Interestingly, CAB has been shown to improve endothelial function in association with CRP decreases in the coronary circulation (*29*). In the present study, the decrease in CRP levels after benidipine treatment may suggest an improvement in vascular function that could have been of some benefit to the patients.

In conclusion, we have confirmed the influence of BP on baPWV in patients undergoing anti-hypertensive therapy. In that context, benidipine relieved arterial stiffness after long-term reduction in BP. Monitoring baPWV in hypertensive patients is convenient and provides useful information about the state of the arterial wall, and with further study may be applicable to estimation of cardiovascular risk.

References

1. Laurent S, Boutouyrie P, Asmar R, *et al*: Aortic stiffness is an independent predictor of all-cause and cardiovascular mortality in hypertensive patients. *Hypertension* 2001; **37**: 1236–1241.
2. Blacher J, Asmar R, Djane S, London GM, Safar ME: Aortic pulse wave velocity as a marker of cardiovascular risk in hypertensive patients. *Hypertension* 1999; **33**: 1111–1117.
3. Guerin AP, Blacher J, Pannier B, Marchais SJ, Safar ME, London ME: Impact of aortic stiffness attenuation on survival of patients in end-stage renal failure. *Circulation* 2001; **103**: 987–992.
4. Kita T, Kitamura K, Hashida S, Morishita K, Eto T: Plasma adrenomedullin is closely correlated with pulse wave velocity in middle-aged and elderly patients. *Hypertens Res* 2003; **26**: 887–893.
5. Imanishi R, Seto S, Toda G, *et al*: High brachial-ankle pulse wave velocity is an independent predictor of the presence of coronary artery disease in men. *Hypertens Res* 2004; **27**: 71–78.
6. Koji Y, Tomiyama H, Ichihashi H, *et al*: Comparison of ankle-brachial pressure index and pulse wave velocity as markers of the presence of coronary artery disease in subjects with a high risk of atherosclerotic cardiovascular disease. *Am J Cardiol* 2004; **94**: 868–872.
7. Munakata M, Ito N, Nunokawa T, Yoshinaga K: Utility of automated brachial ankle pulse wave velocity measurements in hypertensive patients. *Am J Hypertens* 2003; **16**: 653–657.
8. Matsui Y, Kario K, Ishikawa J, Eguchi K, Hoshide S, Shimada K: Reproducibility of arterial stiffness indices (pulse wave velocity and augmentation index) simultaneously assessed by automated pulse wave analysis and their associated risk factors in essential hypertensive patients. *Hypertens Res* 2004; **27**: 851–857.
9. Munakata M, Sakuraba J, Tayama J, *et al*: Higher brachial-ankle pulse wave velocity is associated with more advanced carotid atherosclerosis in end-stage renal disease. *Hypertens Res* 2005; **28**: 9–14.
10. Ichihara A, Hayashi M, Koura Y, Toda Y, Hirota N, Saruta T: Long-term effects of intensive blood pressure lowering on arterial wall stiffness in hypertensive patients. *Am J Hypertens* 2003; **16**: 959–965.
11. Munakata M, Nagasaki A, Nunokawa T, *et al*: Effects of valsartan and nifedipine coat-core on systemic arterial stiffness in hypertensive patients. *Am J Hypertens* 2004; **17**: 1050–1055.
12. Agata J, Nagahara D, Kinoshita S, *et al*: Angiotensin II receptor blocker prevents increased arterial stiffness in patients with essential hypertension. *Circ J* 2004; **68**: 1194–1198.
13. Pitt B, Byington RP, Furberg CD, *et al*, PREVENT Investigators: Effect of amlodipine on the progression of atherosclerosis and the occurrence of clinical events. *Circulation* 2000; **102**: 1503–1510.
14. Zanchetti A, Bond MG, Henning M, *et al*: Calcium antagonist lacidipine slows down progression of asymptomatic carotid atherosclerosis: principal results of the European

Lacidipine Study on Atherosclerosis (ELSA), a randomized, double-blind, long-term trial. *Circulation* 2002; **106**: 2422–2427.
15. Nissen SE, Tuzcu EM, Libby P, *et al*: Effect of antihypertensive agents on cardiovascular events in patients with coronary disease and normal blood pressure: the CAMELOT study: a randomized controlled trial. *JAMA* 2004; **292**: 2217–2225.
16. Dohi Y, Kojima M, Sato K: Benidipine improves endothelial function in renal resistance arteries of hypertensive rats. *Hypertension* 1996; **28**: 58–63.
17. Kobayashi N, Kobayashi K, Kouno K, Yagi S, Matsuoka H: Effect of benidipine on microvascular remodeling and coronary flow reserve in two-kidney, one clip Goldblatt hypertension. *J Hypertens* 1997; **15**: 1285–1294.
18. Yamashita T, Kawashima S, Ozaki M, *et al*: A calcium channel blocker, benidipine, inhibits intimal thickening in the carotid artery of mice by increasing nitric oxide production. *J Hypertens* 2001; **19**: 451–458.
19. Wilkinson IB, Mohammad NH, Tyrrell S, *et al*: Heart rate dependency of pulse pressure amplification and arterial stiffness. *Am J Hypertens* 2002; **15**: 24–30.
20. Benetos A, Adamopoulos C, Bureau J-M, *et al*: Determinants of accelerated progression of arterial stiffness in normotensive subjects and in treated hypertensive subjects over 6-year period. *Circulation* 2002; **105**: 1202–1207.
21. National Intervention Cooperative Study in Elderly Hypertension Study Group: Randomized double-blind comparison of a calcium antagonist and a diuretic in elderly hypertensives. *Hypertension* 1999; **34**: 1129–1133.
22. Tsukiyama H, Kikawada R, Osada H, *et al*: Safety and efficacy of long-term therapy with benidipine in aged hypertensive patients. *Geriat Med* 1997; **35**: 989–1007 (in Japanese).
23. Ito A, Fukumoto Y, Shimokawa H: Changing characteristics of patients with vasospastic angina in the era of new calcium channel blockers. *J Cardiovasc Pharmacol* 2004; **44**: 480–485.
24. Hayashi K, Ozawa Y, Fujiwara K, Wakino S, Kumagai H, Saruta T: Role of actions of calcium antagonists on efferent arterioles—with special references to glomerular hypertension. *Am J Nephrol* 2003; **23**: 229–244.
25. Kobayashi N, Nakano S, Mori Y, Kobayashi T, Tsubokou Y, Matsuoka H: Benidipine inhibits expression of ET-1 and TGF-β1 in Dahl salt-sensitive hypertensive rats. *Hypertens Res* 2001; **24**: 241–250.
26. Yasunari K, Maeda K, Nakamura M, Watanabe T, Yoshikawa J: Benidipine, a long-acting calcium channel blocker, inhibits oxidative stress in polymorphonuclear cells in patients with essential hypertension. *Hypertens Res* 2005; **28**: 107–112.
27. Pai JK, Pischon T, Ma J, *et al*: Inflammatory markers and the risk of coronary heart disease in men and women. *N Engl J Med* 2004; **351**: 2599–2610.
28. Ridker PM, Cannon CP, Morrow D, *et al*: C-reactive protein levels and outcomes after statin therapy. *N Engl J Med* 2005; **352**: 20–28.
29. Takase H, Toriyama T, Sugiyama M, *et al*: Effect of nifedipine on C-reactive protein levels in the coronary sinus and on coronary blood flow in response to acetylcholine in patients with stable angina pectoris having percutaneous coronary intervention. *Am J Cardiol* 2005; **95**: 1235–1237.

ELSEVIER

Cardiovascular Research 70 (2006) 158 – 164

Cardiovascular Research

www.elsevier.com/locate/cardiores

Adrenomedullin in mast cells of abdominal aortic aneurysm

Toshihiro Tsuruda [a,b,*], Johji Kato [a], Kinta Hatakeyama [c], Atsushi Yamashita [c], Kunihide Nakamura [d], Takuroh Imamura [a], Kazuo Kitamura [a], Toshio Onitsuka [d], Yujiro Asada [c], Tanenao Eto [a]

[a] *First Department of Internal Medicine, Miyazaki Medical College, University of Miyazaki, Japan*
[b] *Department of Nutrition Management, Faculty of Health and Nutrition, Minami-Kyushu University, Japan*
[c] *Department of Pathology, Miyazaki Medical College, University of Miyazaki, Japan*
[d] *Second Department of Surgery, Miyazaki Medical College, University of Miyazaki, Japan*

Received 24 September 2005; received in revised form 26 January 2006; accepted 1 February 2006
Available online 9 March 2006
Time for primary review 22 days

Abstract

Objectives: Produced by vascular walls, adrenomedullin (AM) exerts antifibrotic actions in the process of cardiovascular remodeling. The purpose of this study was to examine the pathophysiological role of AM in the development of human abdominal aortic aneurysm (AAA).
Methods and results: Immunohistochemical analyses revealed that vascular smooth muscle cells in the media were positive for AM in the early stage of atherosclerotic aorta. Intense immunoreactivity was observed in mast cells of the outer media and adventitia of AAA, and the number of mast cells was greater ($p<0.01$) in AAA than in atherosclerotic aorta without any aneurysmal change. To determine the role of AM in mast cells, we examined cultured human mast cell leukemia line-1 (HMC-1) and fibroblasts isolated from AAA patients. Cultured HMC-1 cells were found to express preproAM gene and release AM peptide into the cultured media. When assessed by collagenase-sensitive [^{3}H]proline incorporation and procollagen type I C-peptide secretion, collagen synthesis in co-culture of HMC-1 and the fibroblasts was reduced by 10^{-6} mol/L synthetic AM, while conversely, it increased following blockade of the action of endogenous AM with 10 μg/mL anti-AM monoclonal antibody.
Conclusion: The present study suggests an anti-fibrotic role for AM released from mast cells, providing new insight into the biological actions of mast cell-derived AM in the development of AAA.

Keywords: Adrenomedullin; Abdominal aortic aneurysm; Mast cell; Fibrosis

1. Introduction

Abdominal aortic aneurysm (AAA) is a relatively common disorder in elderly patients with atherosclerosis [1,2]. AAA is characterized by an enlarged aortic lumen with a degenerated medial layer that is rearranged by disorganized collagen fibers, and in addition, either fibroblast proliferation with extracellular matrix formation or chronic inflammatory cellular infiltration is often observed in the outer media and adventitia [3]. A number of factors have been proposed as the cause of AAA [4–6]; however, the mechanisms underlying the development of the aneurysm remain unknown.

Adrenomedullin (AM), a 52-amino acid peptide originally isolated from human pheochromocytoma [7], has been shown to exert a wide range of cardiovascular actions, which are mostly protective for blood vessels, such as stimulation of nitric oxide production and inhibitions of oxidative stress and endothelial cell apoptosis [8]. Expression of the AM peptide was observed in the myocardium and in the vascular wall [9], suggesting a role for AM as a locally-acting humoral factor [10,11]. The magnitude of fibrosis of the cardiac or vascular tissues is determined by

* Corresponding author. First Department of Internal Medicine, Miyazaki Medical College, University of Miyazaki, 5200 Kihara Kiyotake, Miyazaki 889-1692, Japan. Tel.: +81 985 85 0872; fax: +81 985 85 6596.
E-mail address: ttsuruda@med.miyazaki-u.ac.jp (T. Tsuruda).

0008-6363/$ - see front matter © 2006 European Society of Cardiology. Published by Elsevier B.V. All rights reserved.
doi:10.1016/j.cardiores.2006.02.003

not only the mechanical stress but also the balance of humoral factors [12]. We have so far reported inhibitory effects of AM on fibroblast proliferation and extracellular matrix formation using cultured cells in vitro [13,14] and rodent models for hypertensive heart disease and myocardial infarction in vivo [15,16]. Based upon previous studies, we hypothesized that AM is involved in the development of AAA through modulation of fibroblast proliferation or extracellular matrix formation.

In the first part of the present study, to examine the role of AM in AAA, we characterized its expression in the aneurysmal aorta obtained from patients with AAA on surgical repair, and found that AM was present in mast cells in the outer media and adventitia. In the second part, we explored whether or not mast cell-derived AM modulates production of the extracellular matrix, by using a human mast cell line and cultured human fibroblasts isolated from the AAA tissue.

2. Materials and methods

The present study is approved by the Human Investigation Review Committee of the University of Miyazaki (Nos. 99 and 177) and conforms with the principles outlined in the Declaration of Helsinki (*Cardiovasc Res* 1997; 35: 2–4).

2.1. Reagents

Synthetic human AM was purchased from Peptide Institute, Inc. (Osaka, Japan). Dulbecco's modified Eagle's medium (DMEM)/F-12, Iscove's modified Dulbecco's medium, fetal bovine serum and antibiotics were obtained from GIBCO BRL. Collagenase (type IV) and insulin-transferrin-sodium selenite media supplement were from Sigma.

2.2. Tissue preparation

Aneurysmal tissues was obtained from the anterior part of aortic walls of 28 patients with AAA associated with atherosclerosis (75±1 years; male, 71%) during elective repair surgery with written informed consent. The AAA tissues were fixed in 10% formalin immediately after resection. Aortic tissues with various degrees of atherosclerosis were collected from the anterior part of aorta of 20 patients (64±3 years; male, 80%) at autopsy performed within 6 h post-mortemly. Tissues of 10 of them showed diffuse intimal thickening or fatty streak and those of 10 advanced atherosclerosis.

2.3. Cell culture

Cultured fibroblasts were isolated from aorta of patients with AAA as described previously with minor modification [13]. In brief, minced aortic tissues digested with 0.12% trypsin and 0.03% collagenase type IV were placed in DMEM/F-12 medium with 10% fetal bovine serum in 10-cm culture plates for 2 h at 37 °C, and the adherent cells were further incubated until confluent. The human mast cell leukemia line, HMC-1, was kindly provided by Dr. J.H. Butterfield (Mayo Clinic, Rochester, MN, USA) [17] and cultured in Iscove's modified Dulbecco's medium.

2.4. Immunohistochemical analysis

Aortic tissues fixed in 10% formalin and embedded in paraffin wax. Sections (3 μm thick) were immunohistochemically examined as previously described [18], with monoclonal antibodies against human α-smooth muscle actin or tryptase (DAKO cytomation) or with anti-human AM monoclonal antibody [19,20]. For detection of mast cell tryptase, the tissue sections were microwaved at 95 °C for 1.0 h in 10 mmol/L citrate buffer (pH 6.0) prior to incubation with the primary antibody. As a negative control, non-immune IgG of mouse was used instead of the primary antibodies. Mast cell numbers of at least 6 fields in total areas of the outer-media and adventitia in atherosclerosis and AAA were counted at the magnification of ×400 and expressed as a density of mast cell number per mm^2. The intracellular localization of AM and tryptase in HMC-1 cells was evaluated by double immunofluorescence staining with the anti-human AM antibody and goat anti-human tryptase polyclonal antibody (Santa Cruz Biotechnology) overnight at 4 °C, followed by staining with fluorescein isothiocyanate-conjugated anti-mouse IgG and Cy3-conjugated anti-goat IgG (Jackson ImmunoResearch) for 20 min. Immunofluorescent images were analyzed with a spectral confocal scanning system (TCS SP2, Leica).

2.5. Gene expression and assay for AM

Gene expression of AM in total RNA isolated from HMC-1 was analyzed by using a reverse transcription-polymerase chain reaction (RT-PCR) method [15,21]. The amplification protocol was 94 °C for 2 min, then 26 cycles of 94 °C for 30 s, 62 °C for 30 s and 72 °C for 1 min, and finally 72 °C for 5 min. The PCR products were electrophoresed on 3.0% agarose gel with ethidium bromide. The concentration of AM in the conditioned medium as well as in the cells was measured with an immunoenzymometric assay, as previously described [22].

2.6. Measurement of collagen synthesis de novo

The synthesis of collagen de novo was assessed by collagen-sensitive proline incorporation into the cells [23,24] and by procollagen type I C-peptide (PICP), a peptide cleaved from the carboxy terminus of procollagen type I during posttranslational processing into the collagen fibers [25], in the conditioned medium. After the confluent fibroblasts were incubated with serum-free DMEM/F-12

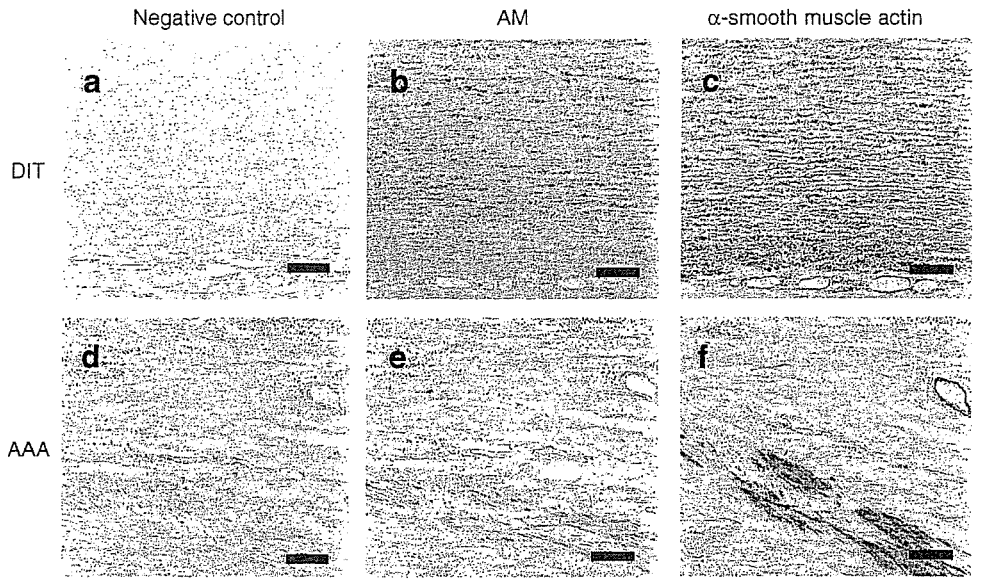

Fig. 1. Localization of immunoreactive AM (b and e) or α-smooth muscle actin (c and f) and negative control (a and d) of aortic tissues with AAA (d–f) and with diffuse intimal thickening (DIT, a–c). Bar, 100 μm.

medium for 48 h, HMC-1 cells (1×10^6/cm^3) were placed on the fibroblasts with or without of 10^{-6} mol/L synthetic AM in the absence or presence of 10 μg/mL purified anti-AM monoclonal antibody or purified non-immune mouse IgG (Zymed Laboratories, Inc., San Francisco, USA). To measure collagen-sensitive proline incorporation, the cultured cells were incubated with 5.0 μCi/mL of [^{3}H]proline (Amersham Bioscience) for a further 24 h. The concentrations of PICP secreted in the conditioned media during the 24-h incubation with or without synthetic AM or anti-AM antibody were determined with commercially available enzyme immunoassay (Takara).

2.7. Statistical analysis

All data were analyzed with the SPSS software of version 11.0 (SPSS Inc., Chicago, IL) and expressed as the median with the 10–90% range and extreme values. Two data were

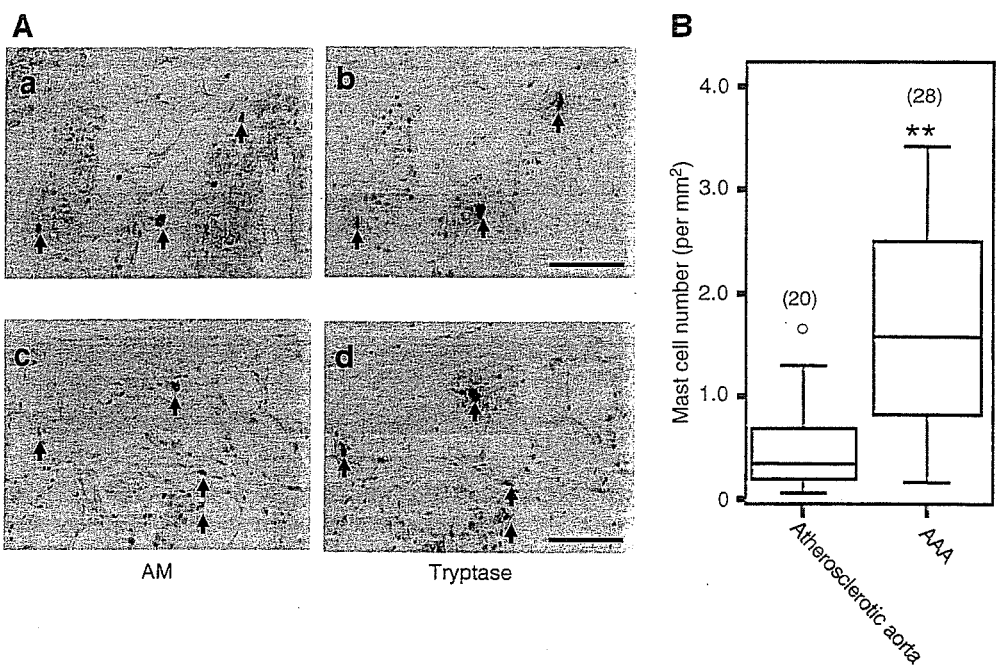

Fig. 2. (A) Localization of immunoreactive AM (a and c) and tryptase (b and d) of two serial sections of AAA. Arrows indicate mast cells positive for AM or tryptase. Bar, 100 μm. (B) Number of mast cells in atherosclerotic aorta and AAA. Mast cells immunostained with anti-human mast cell tryptase antibody were counted at magnification of ×400 under the microscope. Values are shown as the median with 10–90% range (n); $^{**}p < 0.01$, vs. atherosclerotic aorta.

compared with Student's t-test, and comparisons among multiple groups were assessed with a one-way ANOVA followed by Sheffè's test. Statistical significance was accepted at $p<0.05$.

3. Results

3.1. Localization of immunoreactive AM

Fig. 1 illustrates the immunoreactive localization for AM and α-smooth muscle actin in the aortic walls of AAA or of diffuse intimal thickening. In the aneurysmal wall, immunoreactivity for AM was detected in the degenerated media replaced by fibrous tissues, where the residual smooth muscle cells, mural vessels, and fibroblast-like cells were weakly stained. In the aortic wall with diffuse intimal thickening, immunoreactivity for AM was located mainly in the media.

3.2. Immunoreactivity for AM in mast cells of AAA

We further examined the aortic sections from AAA patients stained with anti-AM monoclonal antibody. Fig. 2A illustrates the representative localizations of immunoreactive AM and tryptase in the adventitia of AAA. The immunoreactivity for AM was abundantly present in the cells located in connective tissue, which were identified as mast cells in the serial sections, based on positive staining for tryptase, a specific marker for mast cells. Next, a comparison was made of the number of mast cells between the aortic tissues with and without AAA. As shown in Fig. 2B, the number of mast cells was significantly ($p<0.01$) increased in the outer media and adventitia in cases of AAA, compared to atherosclerotic aorta without AAA.

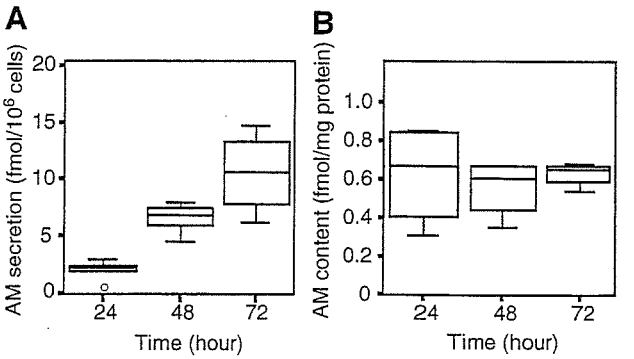

Fig. 4. (A) Secretion of AM from HMC-1 cells into the conditioned media. (B) Intracellular concentration of AM in HMC-1 cells. HMC-1 cells were cultured in serum-free media for the indicated time period. Values are shown as the median with 10–90% range and the numbers of samples are 4–7 for secretion and 4 for AM content measurements.

3.3. AM production in mast cell line

We examined the human mast cell leukemia line HMC-1 to see whether or not mast cells can produce and secrete AM. RT-PCR revealed expression of the preproAM gene in cultured HMC-1 cells (Fig. 3A), and immunohistochemical studies showed that AM (green) and tryptase (red) were positive in a granular pattern, co-localizing partially in merging images (yellow) (Fig. 3B). As shown in Fig. 4A, HMC-1 cells secreted AM into the medium in a time-dependent manner for up to 72 h, with unchanged intracellular AM levels (Fig. 4B). To examine the molecular forms of secreted AM, we analyzed immunoreactive AM secreted from co-culture of the mast cells and fibroblasts over an incubation period of 24 h with reverse phase high-performance liquid chromatography (RP-HPLC). The RP-HPLC analysis showed that immunoreac-

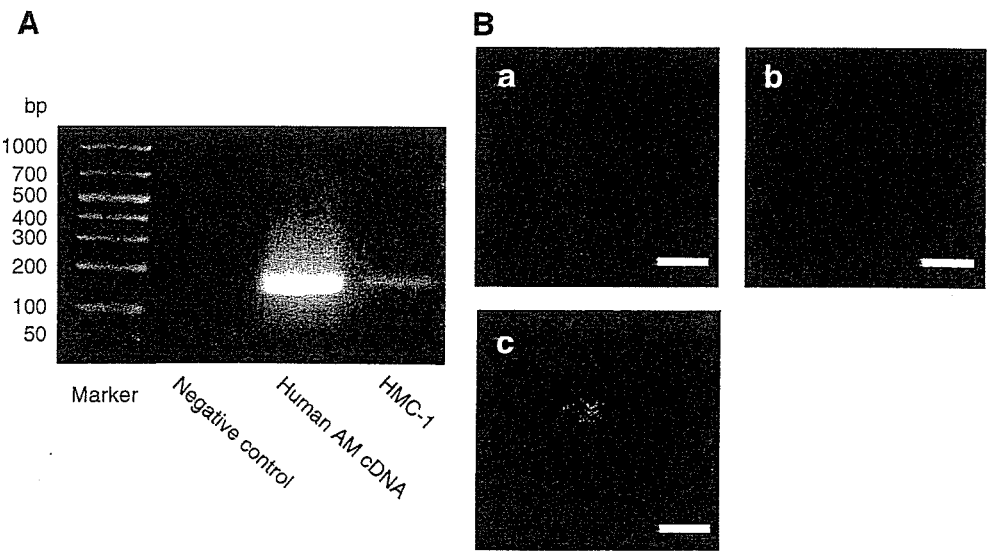

Fig. 3. (A) Expression of preproAM mRNA in the HMC-1 cell line. (B) Localization of immunoreactive AM (a, green) or tryptase (b, red) and a merged image (c, yellow) in HMC-1 cells. Bar, 10 μm.

tive AM consisted of a single peak eluting at the position of human AM(1–52)-NH_2.

3.4. Effect of AM on protein and collagen synthesis

Fig. 5 shows the effects of exogenous and endogenous AM on collagenase-sensitive proline incorporation (A), PICP level in the conditioned media (B) and cellular protein content (C) of cultured HMC-1 cells and fibroblasts isolated from aorta with AAA. Although AM had little effect on the total protein content, 10^{-6} mol/L AM significantly ($p<0.05$) decreased the proline incorporation and PICP level in co-culture of HMC-1 and fibroblasts. In contrast, blockade of the action of endogenous AM with 10 μg/mL of purified anti-AM monoclonal antibody resulted in increased proline incorporation and PICP level.

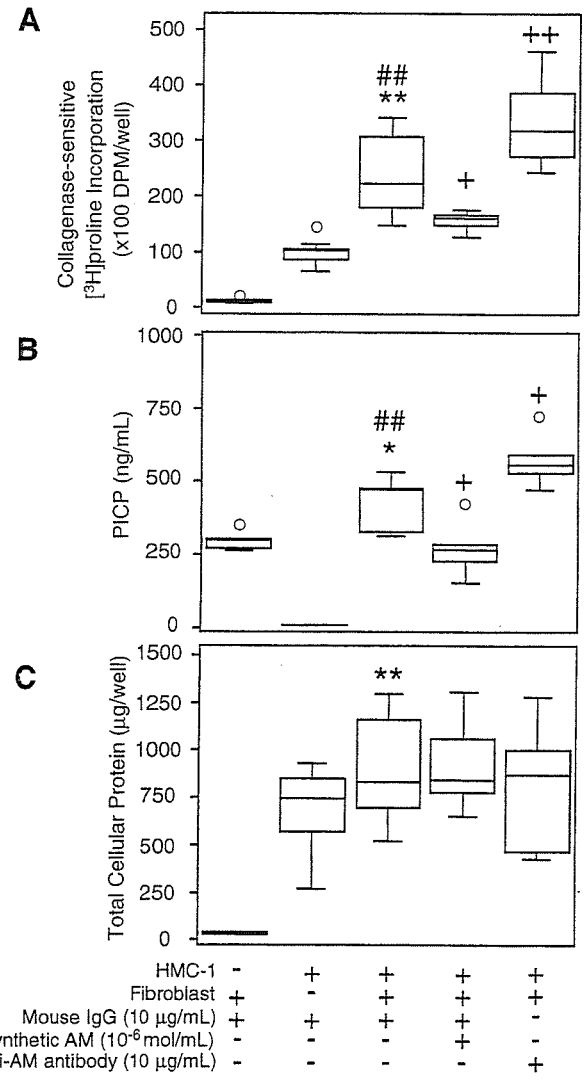

Fig. 5. [^{3}H]proline incorporation (A), procollagen type I C-peptide (PICP) (B) and cellular protein levels (C) of co-culture of HMC-1 cells and fibroblasts incubated with or without 10^{-6} mol/L synthetic AM in the absence or presence of 10 μg/mL purified anti-AM monoclonal antibody or 10 μg/mL purified non-immune mouse IgG. *Values are shown as the median with 10–90% range*, and the number of samples are 8–12 for proline incorporation, 6 for PICP and 6 for cellular protein. $^{*}p<0.05$, $^{**}p<0.01$, vs. fibroblasts alone; $^{\#\#}p<0.01$, vs. HMC-1 alone; $^{+}p<0.05$, $^{++}p<0.01$ vs. control co-culture of fibroblasts and HMC-1 cells.

4. Discussion

Here, we demonstrated the presence of AM in mast cells of the outer media and adventitia of patients with AAA as well as in the human mast cell line HMC-1. Second, AM was released from HMC-1 and suppressed the synthesis of collagen in co-culture of HMC-1 cells and fibroblasts in vitro. The present study suggests a role for mast cell-derived AM in modulating production of the extracellular matrix of AAA.

AM has been reported to be found in various tissues and organs [9], but in particular, locally produced AM in the heart and vasculature has gained attention because of its role as an autocrine or paracrine factor [10,11]. AM exerted anti-fibrotic effects on the heart and blood vessels in vitro and in vivo, attenuating myofibroblastic differentiation and collagen synthesis and stimulating matrix metalloproteinase-2 (MMP-2) activity [14,15]. In the present study, the medial and adventitial layers of the aortic aneurysmal wall were replaced by fibrous tissue, where the residual smooth muscle cells and fibroblast-like cells were weakly positive for AM. Unexpectedly, during the microscopic observation, intense immunoreactivity for AM was observed in mast cells, number of which markedly increased in the outer media and adventitia of AAA. In accord with this, the cultured mast cell line was found to express preproAM mRNA and to contain the AM peptide in the secretory granules.

Accumulation of mast cells is observed in fibrotic tissues of idiopathic cardiomyopathy [26] and of vascular walls with atherosclerotic changes [27], suggesting a potential role of this type of cells in the pathogenesis. Mast cells can directly exert fibrogenic effects by releasing or activating several mediators such as histamine and tryptase [28,29]. To look at the role of AM on extracellular matrix formation in the aneurysmal walls, we treated co-culture of the mast cells and fibroblasts with synthetic AM or purified anti-AM monoclonal antibody which binds to the ring structure, critical for the biological activity of this peptide. When assessed with collagenase-sensitive proline incorporation and with PICP secretion, collagen synthesis de novo in the cells was reduced by synthetic AM, while conversely, increased by the blockade of action of endogenous AM by the anti-AM antibody. These results clearly suggest an inhibitory action of exogenous and endogenous AM on collagen synthesis in the cultured cells. The intracellular mechanisms of action for AM are not completely understood, while accumulation of intracellular cAMP has been proposed as a mechanism [7,8]. Indeed, AM has been shown to inhibit collagen synthesis via elevation of cAMP levels in cultured fibroblasts [30] and this mechanism is

considered for the AM action observed in the present cell-culture study.

Collagen deposition in tissues is determined not only by its production but also by enzymatic degradation, and AM was found to augment MMP-2 activity in cultured aortic adventitial fibroblasts of rats [14]. We therefore measured MMP-2 activity in conditioned media of the mast cells and fibroblasts, but found that neither synthetic AM nor anti-AM antibody had effect on the enzymatic activity (data not shown). Recently, Martínez et al. [31] reported cleavage of the AM peptide into smaller fragments by MMP-2; however RP-HPLC analysis showed that the major molecular form of AM secreted from the mast cells and fibroblasts was the full-length human AM(1–52)-NH_2. Therefore, it seems unlikely that the anti-fibrotic effect of exogenous or endogenous AM is modulated by alteration of MMP-2 activity.

The clinical significance of mast cells in the development of AAA has yet to be defined, though several studies have shown possible activation of chymase and matrix metalloproteinases by the cells [32,33]. In the present study, we observed a significant increase in mast cell number in the outer media and adventitia of AAA. As mentioned above, mast cells are assumed to release pro-fibrotic factors, compensating for the loss of structural integrity in the aneurysmal wall. According to the present experiments in vitro, AM released from mast cells may have potency to suppress deposition of extracellular matrix; however, it is unclear whether or not suppressed extracellular matrix formation by AM is beneficial in preventing AAA from enlarging. *Indeed, we found no significant correlation between the AM levels and collagen contents or wall thickness of the AAA tissues (data not shown), partly because of the limited number of samples or of the removal of intima or part of media during the operation.* Thus, further studies, particularly in vivo, are needed to answer this important question.

In summary, AM was found to be produced by mast cells in the outer media and adventitia of AAA, and the cell culture experiments showed an anti-fibrotic action of AM released from a human mast cell line. This study provides new insight into the biological action of mast cell-derived AM in modulating formation of the extracellular matrix in the development of AAA.

Acknowledgements

This study was supported by grants-in-aid for Scientific Research on Priority Areas and for the 21st Century Centers of Excellence Program (Life Science) from the Ministry of Education, Culture, Sport, Science and Technology, Japan, a grant-in-aid from the Suzuken Memorial Foundation, the Mochida Memorial Foundation for Medical and Pharmaceutical Research, and an incentive grant from Minami-Kyushu University. We are thankful to Dr. J.H. Butterfield, Mayo Clinic, Rochester, MN, USA for providing the mast cell line HMC-1. We also thank Drs. Kazushi Kojima, Mitsuhiro Yano, Yoshikazu Yano, Second Department of Surgery for their help to collect the AAA samples, Drs. Fukumi Nakamura-Uchiyama and Yukifumi Nawa, Department of Parasitology, Dr. Kousuke Marutsuka, Department of Pathology, University of Miyazaki for their helpful discussion, and Ms. Ritsuko Sotomura and Ms. Mariko Tokashiki for their technical assistance.

References

[1] Hallett Jr JW. Management of abdominal aortic aneurysms. Mayo Clin Proc 2000;75:395–9.
[2] Brady AR, Fowkes FG, Thompson SG, Powell JT. Aortic aneurysm diameter and risk of cardiovascular mortality. Arterioscler Thromb Vasc Biol 2001;21:1203–7.
[3] Rosai J. Cardiovascular system. In: Rosai, editor. Rosai and Ackerman's surgical pathology, 9th ed. Philadelphia: Elsevier Inc; 2004. p. 2438–9.
[4] Lindholt JS, Støvring J, Østergaard L, Urbonavicius S, Henneberg EW, Honoré B, et al. Serum antibodies against Chlamydia pneumoniae outer membrane protein cross-react with the heavy chain of immunoglobulin in the wall of abdominal aortic aneurysms. Circulation 2004;109:2097–102.
[5] Freestone T, Turner RJ, Coady A, Higman DJ, Greenhalgh RM, Powell JT. Inflammation and matrix metalloproteinases in the enlarging abdominal aortic aneurysm. Arterioscler Thromb Vasc Biol 1995;15:1145–51.
[6] Leskinen M, Wang Y, Leszczynski D, Lindstedt KA, Kovanen PT. Mast cell chymase induces apoptosis of vascular smooth muscle cells. Arterioscler Thromb Vasc Biol 2001;21:516–22.
[7] Kitamura K, Kangawa K, Kawamoto M, Ichiki Y, Nakamura S, Matsuo H, et al. Adrenomedullin: a novel hypotensive peptide isolated from human pheochromocytoma. Biochem Biophys Res Commun 1993;192:553–60.
[8] Kato J, Tsuruda T, Kita T, Kitamura K, Eto T. Adrenomedullin: a protective factor for blood vessels. Arterioscler Thromb Vasc Biol 2005;12:2480–7.
[9] Eto T, Kato J, Kitamura K. Regulation of production and secretion of adrenomedullin in the cardiovascular system. Regul Pept 2003;112: 61–9.
[10] Kato J, Tsuruda T, Kitamura K, Eto T. Adrenomedullin: a possible autocrine or paracrine hormone in the cardiac ventricles. Hypertens Res 2003;26:S113–9.
[11] Tsuruda T, Burnett Jr JC. Adrenomedullin: an autocrine/paracrine factor for cardiorenal protection. Circ Res 2002;90:625–7.
[12] Weber KT. Targeting pathological remodeling: concepts of cardioprotection and reparation. Circulation 2000;102:1342–5.
[13] Tsuruda T, Kato J, Kitamura K, Kawamoto M, Kuwasako K, Imamura T, et al. An autocrine or a paracrine role of adrenomedullin in modulating cardiac fibroblast growth. Cardiovasc Res 1999;43: 958–67.
[14] Tsuruda T, Kato J, Cao YN, Hatakeyama K, Masuyama H, Imamura T, et al. Adrenomedullin induces matrix metalloproteinase-2 activity in rat aortic adventitial fibroblasts. Biochem Biophys Res Commun 2004;325:80–4.
[15] Tsuruda T, Kato J, Hatakeyama K, Masuyama H, Cao YN, Imamura T, et al. Antifibrotic effect of adrenomedullin on coronary adventitia in angiotensin II-induced hypertensive rats. Cardiovasc Res 2005; 65:921–9.
[16] Nakamura R, Kato J, Kitamura K, Onitsuka H, Imamura T, Cao Y, et al. Adrenomedullin administration immediately after myocardial infarction ameliorates progression of heart failure in rats. Circulation 2004;110:426–31.

[17] Butterfield JH, Weiler D, Dewald G, Gleich GJ. Establishment of an immature mast cell line from a patient with mast cell leukemia. Leuk Res 1988;12:345–55.
[18] Ishikawa T, Hatakeyama K, Imamura T, Ito K, Hara S, Date H, et al. Increased adrenomedullin immunoreactivity and mRNA expression in coronary plaques obtained from patients with unstable angina. Heart 2004;90:1206–10.
[19] Marutsuka K, Hatakeyama K, Sato Y, Yamashita A, Sumiyoshi A, Asada Y. Immunohistological localization and possible functions of adrenomedullin. Hypertens Res 2003;26:S33–40.
[20] Ohta H, Tsuji T, Asai S, Sasakura K, Teraoka H, Kitamura K, et al. One-step direct assay for mature-type adrenomedullin with monoclonal antibodies. Clin Chem 1999;45:244–51.
[21] Uemura T, Kato J, Kuwasako K, Kitamura K, Kangawa K, Eto T. Aldosterone augments adrenomedullin production without stimulating pro-adrenomedullin N-terminal 20 peptide secretion in vascular smooth muscle cells. J Hypertens 2002;20:1209–14.
[22] Kita T, Kitamura K, Hashida S, Morishita K, Eto T. Plasma adrenomedullin is closely correlated with pulse wave velocity in middle-aged and elderly patients. Hypertens Res 2003;26:887–93.
[23] Ostrom RS, Naugle JE, Hase M, Gregorian C, Swaney JS, Insel PA, et al. Angiotensin II enhances adenylyl cyclase signaling via Ca^{2+}/calmodulin. Gq-Gs cross-talk regulates collagen production in cardiac fibroblasts. J Biol Chem 2003;278:24461–8.
[24] Tsuruda T, Boerrigter G, Huntley BK, Noser JA, Cataliotti A, Costello-Boerrigter LC, et al. Brain natriuretic peptide is produced in cardiac fibroblasts and induces matrix metalloproteinases. Circ Res 2002;91:1127–34.
[25] Taubman MB, Goldberg B, Sherr C. Radioimmunoassay for human procollagen. Science 1974;186:1115–7.
[26] Patella V, Marinò I, Arbustini E, Lamparter-Schummert B, Verga L, Adt M, et al. Stem cell factor in mast cells and increased mast cell density in idiopathic and ischemic cardiomyopathy. Circulation 1998; 97:971–8.
[27] Atkinson JB, Harlan CW, Harlan GC, Virmani R. The association of mast cells and atherosclerosis: a morphologic study of early atherosclerotic lesions in young people. Hum Pathol 1994;25:154–9.
[28] Levi-Schaffer F, Piliponsky AM. Tryptase, a novel link between allergic inflammation and fibrosis. Trends Immunol 2003;24:158–61.
[29] Garbuzenko E, Nagler A, Pickholtz D, Gillery P, Reich R, Maquart FX, et al. Human mast cells stimulate fibroblast proliferation, collagen synthesis and lattice contraction: a direct role for mast cells in skin fibrosis. Clin Exp Allergy 2002;32:237–46.
[30] Horio T, Nishikimi T, Yoshihara F, Matsuo H, Takishita S, Kangawa K. Effects of adrenomedullin on cultured rat cardiac myocytes and fibroblasts. Eur J Pharmacol 1999;382:1–9.
[31] Martínez A, Oh HR, Unsworth EJ, Bregonzio C, Saavedra JM, Stetler-Stevenson WG, et al. Matrix metalloproteinase-2 cleavage of adrenomedullin produces a vasoconstrictor out of a vasodilator. Biochem J 2004;383:413–8.
[32] Tsunemi K, Takai S, Nishimoto M, Yuda A, Hasegawa S, Sawada Y, et al. Possible roles of angiotensin II-forming enzymes, angiotensin converting enzyme and chymase-like enzyme, in the human aneurysmal aorta. Hypertens Res 2002;25:817–22.
[33] Baram D, Vaday GG, Salamon P, Drucker I, Hershkoviz R, Mekori YA. Human mast cells release metalloproteinase-9 on contact with activated T cells: Juxtacrine regulation by TNF-α. J Immunol 2001; 167:4008–16.

THE JOURNAL OF BIOLOGICAL CHEMISTRY VOL. 281, NO. 11, pp. 7205–7213, March 17, 2006

Functions of the Cytoplasmic Tails of the Human Receptor Activity-modifying Protein Components of Calcitonin Gene-related Peptide and Adrenomedullin Receptors*[S]

Received for publication, October 13, 2005, and in revised form, January 6, 2006 Published, JBC Papers in Press, January 11, 2006, DOI 10.1074/jbc.M511147200

Kenji Kuwasako[‡1], Yuan-Ning Cao[‡], Chun-Ping Chu[§], Shuji Iwatsubo[‡], Tanenao Eto[‡], and Kazuo Kitamura[‡]

From the [‡]First and [§]Third Departments of Internal Medicine, Miyazaki Medical College, University of Miyazaki, Miyazaki 889-1692, Japan

Receptor activity-modifying proteins (RAMPs) enable calcitonin receptor-like receptor (CRLR) to function as a calcitonin gene-related peptide receptor (CRLR/RAMP1) or an adrenomedullin (AM) receptor (CRLR/RAMP2 or -3). Here we investigated the functions of the cytoplasmic C-terminal tails (C-tails) of human RAMP1, -2, and -3 (hRAMP1, -2, and -3) by cotransfecting their C-terminal deletion or progressive truncation mutants into HEK-293 cells stably expressing hCRLR. Deletion of the C-tail from hRAMP1 had little effect on the surface expression, function, or intracellular trafficking of the mutant heterodimers. By contrast, deletion of the C-tail from hRAMP2 disrupted transport of hCRLR to the cell surface, resulting in significant reductions in ^{125}I-hAM binding and evoked cAMP accumulation. The transfection efficiency for the hRAMP2 mutant was comparable with that for wild-type hRAMP2; moreover, immunocytochemical analysis showed that the mutant hRAMP2 remained within the endoplasmic reticulum. FACS analysis revealed that deleting the C-tail from hRAMP3 markedly enhances AM-evoked internalization of the mutant heterodimers, although there was no change in agonist affinity. Truncating the C-tails by removing the six C-terminal amino acids of hRAMP2 and -3 or exchanging their C-tails with one another had no effect on surface expression, agonist affinity, or internalization of hCRLR, which suggests that the highly conserved Ser-Lys sequence within hRAMP C-tails is involved in cellular trafficking of the two AM receptors. Notably, deleting the respective C-tails from hRAMPs had no effect on lysosomal sorting of hCRLR. Thus, the respective C-tails of hRAMP2 and -3 differentially affect hCRLR surface delivery and internalization.

CGRP[2] and AM belong to the calcitonin family of regulatory molecules and exert a wide variety of biological effects, including potent vasorelaxation (1–3). The receptors that mediate these effects are heterodimers composed of CRLR and RAMP, a novel accessory protein (4). The three RAMP isoforms (RAMP1, RAMP2, and RAMP3) are each composed of ~160 amino acids, and all exhibit a common structure that includes a large extracellular N-terminal domain, a single membrane-spanning domain, and a very short C-tail, but they share less than 30% sequence identity and differ in their tissue distributions (4, 5). When acting as a chaperone, each RAMP forms a 1:1 heterodimer with CRLR, probably in the ER (4, 6). They then mediate the transport of CRLR to the cell surface, where the heterodimers form functional CGRP or AM receptors: CRLR/RAMP1 forms the $CGRP_1$ receptor (4), which can also be activated by high concentrations of AM (7, 8); CRLR/RAMP2 forms an AM-specific receptor that is sensitive to the AM receptor antagonist AM-(22–52) (AM_1 receptor) (7, 9); and CRLR/RAMP3 forms an AM receptor that is sensitive to both the $CGRP_1$ receptor antagonist CGRP-(8–37) and AM-(22–52) (AM_2 receptor) (7, 9). It is the RAMP extracellular domain that mediates agonist binding to CRLR/RAMP heterodimers (11–13), which in turn mediate intracellular cAMP production and Ca^{2+} mobilization (4, 10).

Exposing cells that express GPCRs to their respective agonists frequently leads to a rapid internalization of the receptor in a process believed to involve clathrin-coated vesicles, caveolin-rich vesicles, or both (14, 15). The internalized GPCRs may be recycled back to the plasma membrane in order to promote functional restoration of signal transduction, or they may be trafficked to lysosomes, where they are degraded (14, 15). Similarly, upon binding their respective agonist, hCRLR/RAMP heterodimers stably expressed in HEK-293 cells are rapidly internalized without dissociation via clathrin-coated vesicles (6, 10) in a process that is blocked by dominant negative mutants of dynamin and β-arrestin 2 (6). In that regard, it is well known that G protein-coupled receptor kinases phosphorylate serine/threonine sites located in many GPCR C-tails, enabling β-arrestins to bind there (16). After internalization, both CRLR and RAMP are targeted to lysosomes (10), where they are degraded (6).

Although short, the RAMP C-tails do contain potential sites of interaction with other proteins (5, 17). For instance, the hRAMP3 C-tail possesses a classical type I PDZ (PSD-95/Disc-large/ZO-1) binding motif (TLL) (5, 17), and the binding of NSF to the PDZ motif of hRAMP3 was found to promote slow recycling of internalized hCRLR/hRAMP3 heterodimers in HEK-293 cells (18). In addition, a five-residue motif (QSKRT) in the hRAMP1 C-tail can act as an ER retention signal (19). The C-tails of RAMPs, like that of CRLR, also contain potential phosphorylation and ubiquitination sites (5, 17). Ubiquitination is the post-translational attachment of ubiquitin lysine residues in the substrate proteins (20, 21); it is not crucial for receptor internalization but is essential for proper trafficking to lysosomes for degradation (22, 23). Whether the phosphorylation and ubiquitination sites are also involved

* This work was supported in part by grants-in-aid for scientific research on priority areas and for the 21st Century Centers of Excellence Program (Life Science) from the Ministry of Education, Culture, Sports, Science, and Technology, Japan. The costs of publication of this article were defrayed in part by the payment of page charges. This article must therefore be hereby marked "*advertisement*" in accordance with 18 U.S.C. Section 1734 solely to indicate this fact.

[S] The on-line version of this article (available at http://www.jbc.org) contains one supplemental figure.

[1] To whom correspondence should be addressed. Tel.: 81-985-85-0872; Fax: 81-985-85-6596; E-mail: kuwasako@fc.miyazaki-med.ac.jp.

[2] The abbreviations used are: CGRP, calcitonin gene-related peptide; hαCGRP, human αCGRP; AM, adrenomedullin; hAM, human AM; CRLR, calcitonin receptor-like receptor; hCRLR, human CRLR; RAMP, receptor activity-modifying protein; C-tail, cytoplasmic C-terminal tail; ER, endoplasmic reticulum; GPCRs, G protein-coupled receptors; NSF, *N*-ethylmaleimide-sensitive factor; hNSF, human NSF; PDZ, PSD-95/Disc-large/ZO-1; FITC, fluorescein isothionate; PE, phycoerythrin; HEK, human embryonic kidney; GFP, green fluorescent protein; FACS, fluorescence-activated cell sorting; PBS, phosphate-buffered saline; NHERF, Na^+/H^+ exchanger regulatory factor; β_2-AR, β_2-adrenergic receptor.

in intracellular trafficking of CRLR/RAMP heterodimers remains unknown. To address that issue, we examined the effects of expressing various hRAMP C-tail deletion and progressive truncation mutants and chimeras in which the C-tails were exchanged among the three hRAMPs in HEK-293 cells stably expressing hCRLR.

EXPERIMENTAL PROCEDURES

Materials—^{125}I-[Tyr^0]hαCGRP (specific activity 2 μCi/pmol) (24), which contains an extra N-terminal tyrosine residue (Tyr^0), and ^{125}I-hAM (specific activity 2 μCi/pmol) (1) were both produced in our laboratory. Human αCGRP was purchased from Peptide Institute (Osaka, Japan). [Tyr^0]hαCGRP was from Phoenix Pharmaceuticals, Inc. Human AM was kindly donated by Shionogi & Co. (Osaka, Japan). Mouse anti-hNSF antibody was from Calbiochem. Mouse anti-V5 antibody and FITC-conjugated mouse anti-V5 monoclonal antibody (anti-V5-FITC antibody) were from Invitrogen. Rabbit anti-calnexin antibody was from Stressgen Biotechnologies Corp. (Victoria, Canada), and Alexa Fluor® 594 (biotin- and fluorescent dye-labeled goat anti-rabbit IgG antibody) were from Molecular Probes, Inc. (Eugene, OR). PE-conjugated rabbit anti-mouse secondary antibody was from Exalpha Biologicals, Inc. All other reagents were of analytical grade and were obtained from various commercial suppliers.

Expression Constructs—hNSF (GenBank™ accession number BC030613) was cloned from cDNA obtained from human heart (Clontech) using PCR with the appropriate primers and then modified to provide a consensus Kozak sequence as previously described (25). hRAMP1, -2, and -3 (4) were also modified to provide the same Kozak sequence. A double V5 epitope tag (GKPIPNPLLGLDST) was ligated, in frame, to the 5′-end of the cDNAs encoding each intact hRAMP, and the native signal sequences were removed and replaced with MKTILALSTYIFCLVFA (26), yielding V5-hRAMP1, -2, and -3. The deletion and progressive truncation mutations in the V5-hRAMP C-tails were created by using 3′-primers that introduced a translational stop codon at the desired positions (Fig. 1); with RAMP3, for instance, Δ139 represents a mutant in which a stop codon was introduced after residue 139. In addition, various V5-hRAMP chimeras were constructed by exchanging the 9 C-terminal amino acid residues among the three hRAMPs. The hNSF, V5-hRAMPs, V5-hRAMP deletion and truncation mutants, and V5-hRAMP chimeras were then respectively cloned into the mammalian expression vector pCAGGS/Neo (10) using the 5′-XhoI and 3′-NotI sites, and the sequences of the resultant constructs were all verified using an Applied Biosystems 310 Genetic Analyzer. The individual V5-hRAMPs were compared with the native sequence in the assays and were found to behave identically (data not shown).

Cell Culture and DNA Transfection—HEK-293 cells stably expressing a hCRLR-GFP chimera (10) were maintained in Dulbecco's modified Eagle's medium supplemented with 10% fetal bovine serum, 100 units/ml penicillin G, 100 μg/ml streptomycin, 0.25 μg/ml amphotericin B, and 0.25 mg/ml G 418 at 37 °C under a humidified atmosphere of 95% air, 5% CO_2. For experimentation, cells were seeded into 6- or 24-well plates and, upon reaching 70–80% confluence, were transiently cotransfected with the indicated cDNAs using Lipofectamine transfection reagents (Invitrogen) according to the manufacturer's instructions. Briefly, the cells were incubated for 4 h in Opti-MEM I medium containing plasmid DNAs, Plus reagent, and Lipofectamine (see Ref. 27 for 6-well and Ref. 11 for 24-well plates). As a control, some cells were transfected with empty vector (mock). All experiments were carried out 48 h after transfection.

FACS Analysis—Flow cytometry was carried out to assess the levels of cell surface expression of V5-hRAMPs, V5-hRAMP truncation mutants, or V5-hRAMP chimeras in HEK-293 cells. To evaluate cell surface expression, cells were harvested following transient transfection, washed twice with PBS, resuspended in ice-cold FACS buffer (27), and then incubated for 60 min at 4 °C in the dark with anti-V5 monoclonal antibody (1:1000 dilution). Following two additional washes with FACS buffer, the cells were incubated for 60 min at 4 °C in the dark with PE-conjugated rabbit anti-mouse secondary antibody (1:400 dilution) in ice-cold FACS buffer. For evaluation of whole cell expression, cells were first permeabilized using IntraPrep™ reagents (Beckman Coulter, Fullerton, CA) according to the manufacturer's instructions and then incubated with anti-V5-FITC antibody (1:500 dilution) for 15 min at room temperature in the dark. Following two successive washes with FACS buffer, both groups of cells were subjected to flow cytometry in an EPICS XL flow cytometer (Beckman Coulter) and analyzed using EXPO 2 software (Beckman Coulter). Fluorophores were excited at 488 nm, and the emission was monitored at 530 nm for GFP and 575 nm for PE. Viability was assessed by exclusion of propidium iodide.

Immunofluorescence Microscopy—HEK-293 cells stably expressing hCRLR-GFP were plated onto 35-mm glass-bottomed dishes (Iwaki, Tokyo, Japan). As determined by the experimental protocol, some cells were then transiently transfected with V5-hRAMP2, Δ166-hRAMP2, or Δ167-hRAMP2. The cells were then fixed with 3.7% formaldehyde in PBS for 20 min at room temperature, washed twice with PBS, and permeabilized with 0.25% Triton X-100 in PBS for 10 min. Thereafter, the cells were incubated at room temperature for 30 min in blocking buffer (PBS containing 1% bovine serum albumin), followed by incubation for 60 min first with rabbit anti-calnexin (1:200 dilution) and mouse anti-V5-FITC antibody (1:500 dilution) and then, after washing four times with PBS, with the Alexa Fluor® 594 diluted 1:100 in blocking buffer. After another three washes with PBS, the cells were mounted using Slow-Fade mounting medium (Molecular Probes, Inc.), and a 22-mm glass coverslip was seated in the center of each dish. Double labeling was

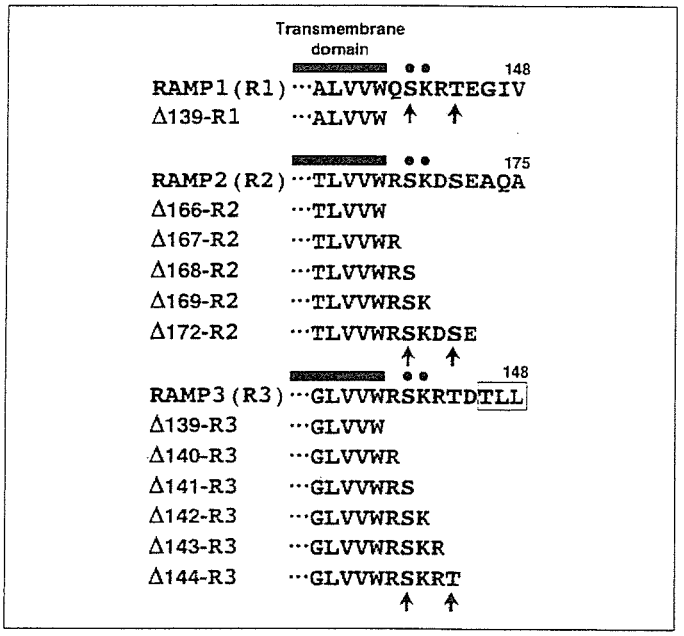

FIGURE 1. **Amino acid sequence alignment of the cytoplasmic tails of hRAMP1, -2, and -3.** The sequences are aligned for maximum homology; alignment of the entire sequences was presented by MacLatchie *et al.* (4). The *numbers* indicate the amino acid positions in accordance with Sexton *et al.* (5). *Black circles* indicate conserved amino acids; *arrows* indicate potential phosphorylation sites; and the PDZ binding motif is *boxed*. The progressive hRAMP C-tail truncation mutants were created using 3′-primers that introduced a translational stop codon at the indicated positions; for instance, Δ139 represents a truncation mutant that introduced a stop codon after residue 139.

viewed using a TCS-SP2 AOBS confocal laser-scanning microscope (Leica) equipped with a × 63/1.32 numerical aperture immersion lens (Leica).

Whole-cell Radioligand Binding Assays—Transfected HEK-293 cells in 24-well plates were washed twice with prewarmed PBS and then incubated for 5 h at 4 °C with ^{125}I-[Tyr^0]hαCGRP (100 pM) or ^{125}I-hAM (20 pM) in the presence (for nonspecific binding) or absence (for total binding) of 1 μM unlabeled hαCGRP or hAM in modified Krebs-Ringer-HEPES medium (10), after which they were washed twice more with ice-cold PBS and harvested with 0.5 M NaOH. The associated cellular radioactivity was measured in a γ-counter. Specific binding was defined as the difference between total binding and nonspecific binding.

cAMP Measurements—Transfectants in 24-well plates were incubated for 15 min at 37 °C in Hanks' buffer containing 20 mM HEPES, 0.2% bovine serum albumin, 0.5 mM 3-isobutyl-1-methylxanthine (Sigma), and the indicated concentrations of hαCGRP or hAM. The reaction mixture was then replaced with 20 mM HCl and 1 M acetic acid to extract the intracellular cAMP, after which the resultant extracts were lyophilized and stored at −30 °C until assayed. The cAMP concentrations were measured using our specific radioimmunoassay (1).

FACS Analysis of Receptor Internalization and Recycling—Following cotransfection of the indicated cDNAs into HEK-293 cells stably expressing hCRLR-GFP in 6-well plates, the cells were exposed to selected concentrations of hαCGRP or hAM in prewarmed serum-free Dulbecco's modified Eagle's medium containing 20 mM HEPES and 0.2% bovine serum albumin for the indicated periods (up to 2 h) at 37 °C. For receptor recycling studies, the cells were incubating for 60 min with the agonist plus 10 μg/ml cycloheximide and 10 μg/ml brefeldin A and then washed three times with prewarmed PBS. The medium was then replaced with prewarmed Dulbecco's modified Eagle's medium containing 20 mM HEPES, 10% fetal bovine serum, 10 μg/ml cycloheximide, and 10 μg/ml brefeldin A for the indicated periods (up to 4 h) at 37 °C. Internalization and recycling were stopped by adding ice-cold PBS, after which the cells were harvested, resuspended in ice-cold FACS buffer, and labeled with anti-V5 monoclonal antibody and fluorescein PE-conjugated rabbit anti-mouse secondary antibody. The cells were then subjected to flow cytometry and analyzed as described above.

mRNA Expression Measured by Real Time Quantitative PCR—Total RNAs were extracted from HEK-293 cells either untransfected or transfected as indicated using total RNA isolation reagent (Invitrogen). Thereafter, the target cDNAs were synthesized from the respective mRNAs by reverse transcription using SuperScript reverse transcriptase (Invitrogen). The expression of mRNAs encoding hNSF was assessed using real time quantitative PCR (Prism 7700 Sequence Detector, Applied Biosystems, Foster City, CA) with original oligonucleotide primers (sense, 5′-AGAACAGTGACCGCACACCAT-3′; antisense, 5′-TCCACAACCACACAACTGAGC-3′) and a fluorescently labeled probe (5′-AGCGTGCTTCTGGAAGGCCCTCCTCACAGT-3′). The size of the amplified DNA was 223 bp. The levels of hNSF mRNA were normalized to those of glyceraldehyde-3-phosphate dehydrogenase mRNA, which served as an internal control.

Western Analysis—Following transient transfection of hNSF into cells plated in 6-well plates, the transfectants were washed twice with ice-cold PBS, harvested in 1 ml of sample buffer (28), and boiled for 10 min. Equal aliquots of protein (20 μg) were then subjected to 10% SDS gel electrophoresis and transferred to a Hybond-P membrane (Amersham Biosciences). The membrane was then blocked with 5% block reagent (Amersham Biosciences), washed, and incubated first for 1 h at room temperature with rabbit anti-hNSF antibody (1:1,000 dilution) and then with secondary antibody (1:10,000 dilution). hNSF proteins were detected using an ECL Plus chemiluminescence kit (Amersham Biosciences), after which they were quantitated by densitometry using Image Gauge (LAS-1000; Fujifilm).

Statistical Analysis—Results are expressed as means ± S.E. of at least three independent experiments. Differences between two groups were evaluated using Student's *t* tests; differences among multiple groups were evaluated with a one-way analysis of variance followed by Scheffe's tests. Values of $p < 0.05$ were considered significant.

RESULTS

Deletion of hRAMP C-tails—We previously established HEK-293 cells stably expressing hCRLR-GFP alone or together with Myc-hRAMPs and used them to visualize the cellular localization and trafficking of hCRLR (10). Following AM exposure, hCRLR is rapidly internalized together with its associated hRAMP, and then both are trafficked to lysosomes; fusion of GFP to the C terminus of hCRLR had no apparent effect on the trafficking of the heterodimeric receptor. In the present study, therefore, we used HEK-293 cells stably expressing hCRLR-GFP to examine the functions of the C-tails of the three hRAMPs within the respective CRLR/RAMP heterodimers.

We initially tested the effect of completely deleting the C-tails of the three V5-epitope tagged hRAMPs (Fig. 2). When coexpressed with hCRLR, V5-RAMP1, -2, and -3 were detected at the surfaces of 45.9, 21.9, and 38.9% of cells, respectively. On the other hand, the V5-RAMP deletion mutants Δ139-RAMP1, Δ166-RAMP2, and Δ139-RAMP3 appeared at the surface of 43.7, 5.0, and 38.8% of cells, respectively. Thus, deletion of the C-tail significantly reduced surface delivery of only RAMP2. Surface immunoreactivity was detected in only 0.55% of cells expressing the empty vector (Mock), which is well within the 2% limit of resolution characteristic of FACS analysis.

We next evaluated the binding profiles of ^{125}I-[Tyr^0]hαCGRP and ^{125}I-hAM to cells expressing each of the wild-type and mutant receptors (Fig. 3, *A* and *B*). When CRLR-GFP was coexpressed with empty vector (*Mock*), the cells showed only very low levels of specific binding of ^{125}I-[Tyr^0]αCGRP and ^{125}I-AM. Co-transfection of RAMP1 led to markedly higher specific ^{125}I-[Tyr^0]αCGRP binding than was seen with Δ139-RAMP1 (Fig. 3*A*), although there was no difference in the surface expression of either heterodimeric receptor (Fig. 2). Likewise, cotransfection of RAMP2 significantly increased the specific binding of

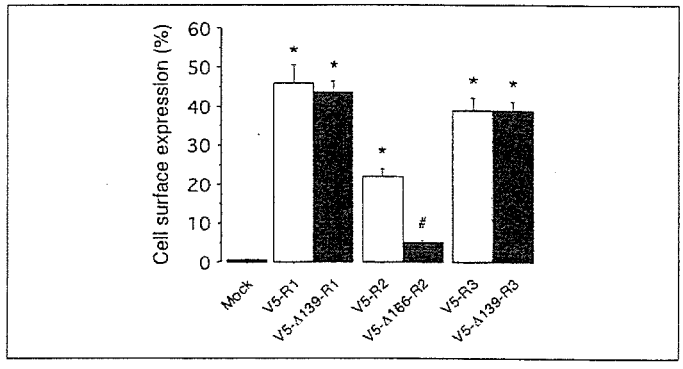

FIGURE 2. **FACS analysis of HEK-293 cells coexpressing hCRLR with intact hRAMP or a C-terminal deletion mutant.** HEK-293 cells stably expressing CRLR-GFP were transiently transfected with empty vector (*Mock*) or the indicated V5-RAMP or deletion mutant. The cells were incubated first with an anti-V5 monoclonal antibody and then with a fluorescein PE-conjugated rabbit anti-mouse secondary antibody. Samples incubated with only secondary antibody served as the control. Cell surface expression of each construct was estimated by flow cytometry. The *bars* represent means ± S.E. of six independent experiments. *, $p < 0.001$ *versus* control (*Mock*); #, $p < 0.02$ *versus* corresponding wild-type V5-RAMP.

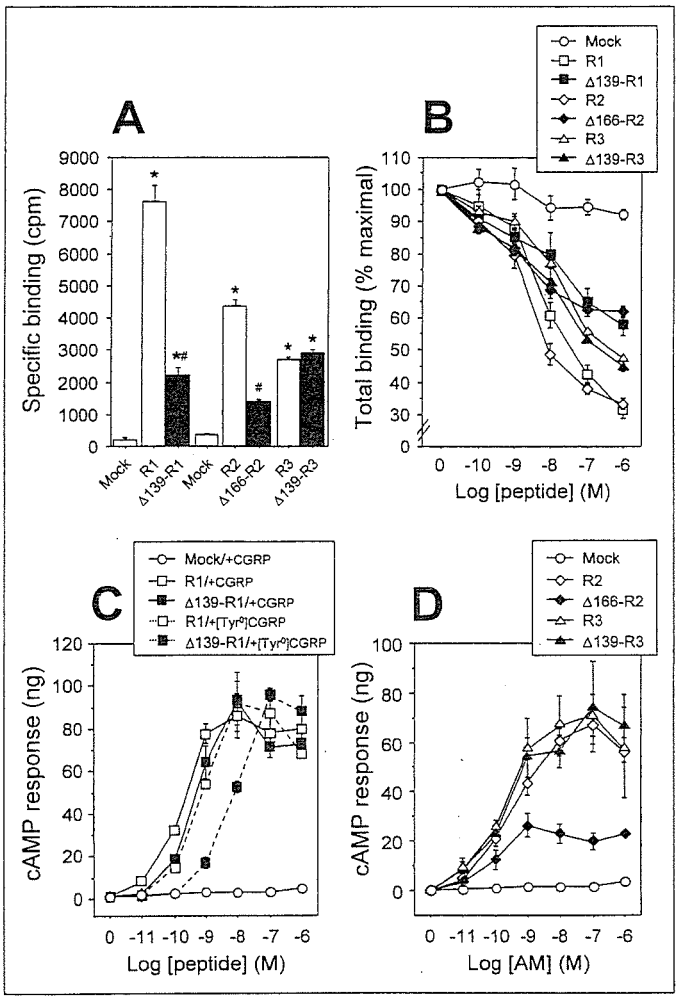

FIGURE 3. **Effects of hRAMP C-terminal deletion on agonist binding and evoked cAMP production in HEK-293 cells stably expressing hCRLR.** *A*, specific binding of ^{125}I-hαCGRP and ^{125}I-hAM. HEK-293 cells expressing CRLR-GFP were transiently transfected with empty vector (*Mock*) or the indicated V5-RAMP or deletion mutant, after which the cells were incubated for 5 h at 4 °C with ^{125}I-αCGRP (100 pM) or ^{125}I-AM (20 pM) in the presence or absence of 1 μM unlabeled αCGRP or AM. *Bars* represent means ± S.E. of three experiments. *, $p < 0.002$ *versus* Mock; #, $p < 0.001$ *versus* corresponding wild-type V5-RAMP. *B*, displacement of radioligand. Cells were transfected and radiolabeled as in *A* either alone or with the indicated concentration of unlabeled ligand (αCGRP or AM). *Bars* represent means ± S.E. of three experiments. *C* and *D*, evoked cAMP production. After transient transfection of V5-RAMPs and the corresponding deletion mutants, cells were exposed to the indicated concentrations of αCGRP, [Tyr^0]αCGRP, or AM for 15 min at 37 °C and then lysed. The resultant lysates were analyzed for cAMP content. *Bars* represent means ± S.E. of three experiments.

^{125}I-AM to CRLR-GFP-expressing cells, whereas cotransfection of Δ166-RAMP2 did not. In this case, the reduced binding could be due to reduced surface delivery of the mutant receptors (Fig. 2). Finally, deletion of the RAMP3 C-tail had no effect on specific ^{125}I-AM binding.

Fig. 3*B* shows a set of ^{125}I-[Tyr^0]αCGRP and ^{125}I-AM competition curves for the wild-type and mutant receptors. The IC_{50} values derived from the curves obtained with cotransfection of Δ139-RAMP1 or Δ166-RAMP2 were both >1000 nM, which is much higher than those for RAMP1 and -2 (43.0 and 12.2 nM, respectively). By contrast, the IC_{50} values obtained with expression of RAMP3 or Δ139-RAMP3 were within the same order of magnitude (560 and 257 nM, respectively).

We then further characterized the mutant receptors by measuring agonist-induced intracellular cAMP accumulation (Fig. 3, *C* and *D*). αCGRP and AM elicited little or no cAMP production in HEK-293 cells expressing CRLR-GFP alone, indicating that the stable transfectants used in this study express no functional RAMP proteins. In cells coexpressing RAMP1 and CRLR-GFP, by contrast, αCGRP (EC_{50} = 0.18 nM) elicited marked increases in cAMP (Fig. 3*C*). In cells expressing Δ139-RAMP1 with CRLR-GFP, the EC_{50} for αCGRP was increased only a little, as compared with RAMP1 (to 0.49 nM), and the maximal responses were also similar to those seen with RAMP1 (Fig. 3*C*). Interestingly, the responses to [Tyr^0]αCGRP by cells expressing CRLR-GFP/Δ139-RAMP1 (EC_{50} = 8.5 nM) were significantly smaller than those seen in cells expressing CRLR-GFP/RAMP1 (EC_{50} = 0.79 nM). In cells transfected with RAMP2, AM elicited significant increases in cAMP (EC_{50} = 0.38 nM), but these responses were diminished by 62.1% in cells transfected with Δ166-RAMP2, although there was no significant change in EC_{50} (0.16 nM) (Fig. 3*D*). AM-evoked cAMP production did not significantly differ in cells expressing RAMP3 or Δ139-RAMP3 (EC_{50} = 0.41 and 0.20 nM, respectively) (Fig. 3*D*). That the cAMP production elicited via the respective receptors largely paralleled the profile of radioligand binding (Fig. 3, *A* and *B*) suggests that the C-tails of RAMP1 and -3 have little or no involvement with agonist binding and signaling.

We previously quantified the internalization and recycling of AM receptors (CRLR/RAMP heterodimers) using radioligand binding assays; however, interpretation of those experiments was complicated by the high degree of nonspecific AM binding, which reflected the highly hydrophobic and basic nature of the native peptide (1, 10, 11). In the present study, therefore, we used FACS to evaluate agonist-mediated internalization and recycling of wild-type and mutant CRLR-GFP/RAMP heterodimers. Fig. 4*A* shows the receptor internalization induced by 1 μM αCGRP- or AM. Exposure to the appropriate agonist elicited rapid declines in cell surface expression of wild-type CRLR-GFP/RAMP1 and -3 that led to 40–60% reductions in signal strength within 2 h and to 90% reduction in cell surface CRLR-GFP/RAMP2 within 30 min. Heterodimers composed of CRLR-GFP plus Δ139-RAMP1 or Δ166-RAMP2 tended to be internalized somewhat less efficiently, whereas internalization of the CRLR-GFP/Δ139-RAMP3 heterodimer was markedly enhanced. Notably, these phenomena occurred with no changes in cell surface CRLR-GFP expression or AM binding and signaling (Figs. 2 and 3).

The dose dependence of the agonist-evoked receptor internalization is illustrated in Fig. 4*B*. αCGRP elicited equivalent dose-dependent internalization of CRLR-GFP/RAMP1 and CRLR-GFP/Δ139-RAMP1. AM dose-dependently induced RAMP2-mediated internalization of CRLR-GFP, which was more efficient than RAMP1-mediated internalization. And Δ166-RAMP2 mediated internalization of CRLR-GFP even more efficiently than did wild-type RAMP2, although the basal surface expression of CRLR-GFP/Δ166-RAMP2 was much lower (Fig. 2*A*). Δ139-RAMP3-mediated internalization of CRLR-GFP only differed from that mediated by wild-type RAMP3 at high AM concentrations (100 nM and 1 μM), at which time internalization of the mutant was more efficient.

Progressive Truncation of the C-Tails of hRAMP2 and -3—The results presented so far show that for hRAMP1, the C-tail is not necessary for cell surface delivery and internalization of CRLR (Figs. 2 and 4). For hRAMP2 and -3, by contrast, the respective C-tails do appear to be involved in determining the surface expression and internalization kinetics of CRLR.

To determine more precisely which sites on the C-tails of hRAMP2 and -3 regulate the cellular trafficking of CRLR/RAMP heterodimers, we constructed a group of progressive C-tail truncation mutants (Fig. 1) and then transfected each RAMP construct into HEK-293 cells stably expressing CRLR-GFP. When Δ166- or Δ167-RAMP2 was individually transfected into HEK-293 cells, its transfection efficiency (~15%) was

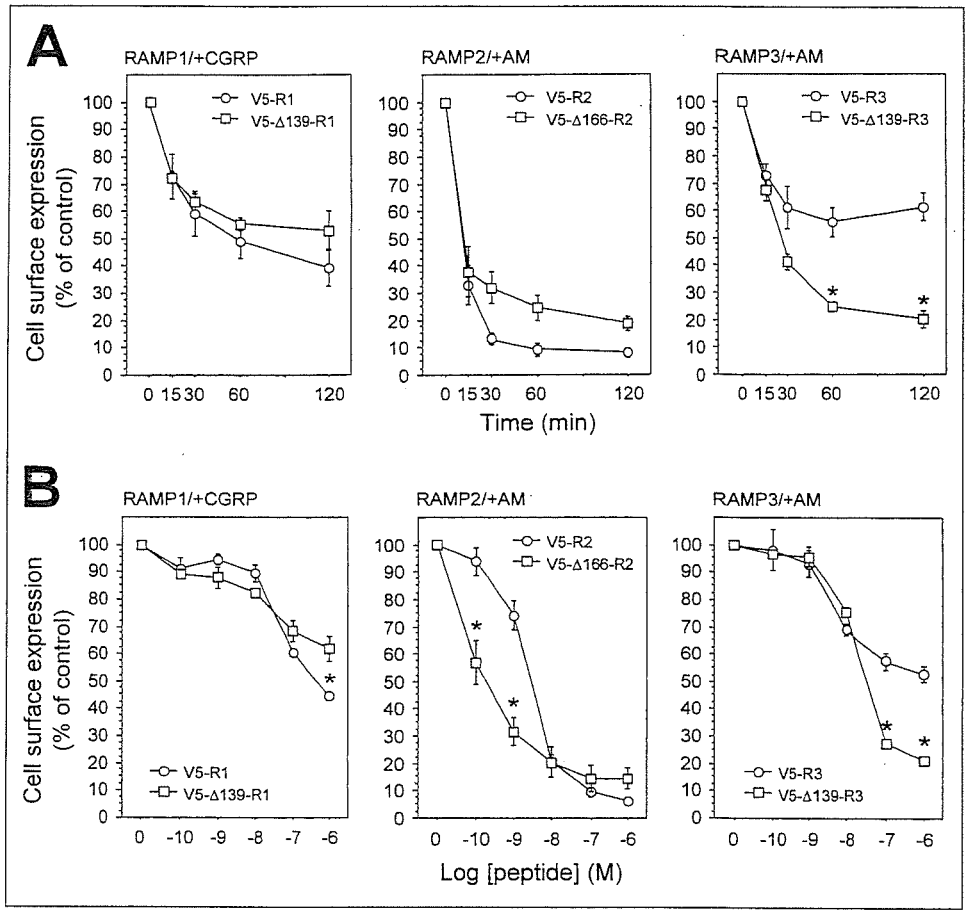

FIGURE 4. **FACS analysis of the time course of agonist-induced internalization of hCRLR with hRAMPs or their C-terminal deletion mutants.** *A*, time-dependent loss of surface CRLR/RAMP heterodimers. HEK-293 cells stably expressing CRLR-GFP were transiently transfected with V5-RAMPs or their C-terminal deletion mutants and then treated with 1 μM αCGRP or AM for the indicated times. Cell surface expression of each construct was estimated by flow cytometry. The *symbols* represent means ± S.E. of three independent experiments; *, $p < 0.006$ *versus* control. *B*, agonist-evoked internalization of hCRLR with hRAMPs or their deletion mutants. Each transfectant was incubated for 60 min with the indicated concentrations of αCGRP or AM. Cell surface expression of each construct was estimated by flow cytometry. *Symbols* represent means ± S.E. of three independent experiments; *, $p < 0.03$ *versus* control.

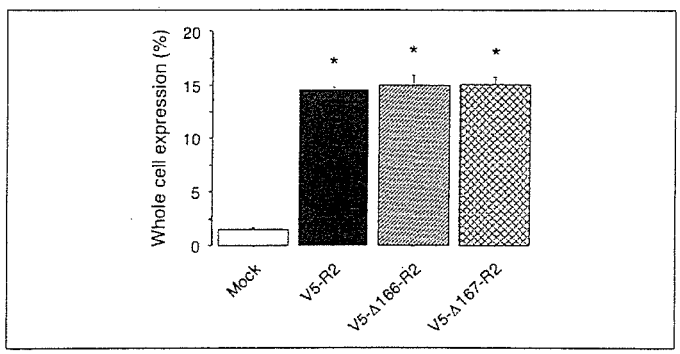

FIGURE 5. **FACS analysis of whole cell expression of hRAMP2 and its truncation mutants.** The indicated RAMP constructs were transiently transfected into HEK-293 cells. Forty-eight hours after transfection, cells were permeabilized with IntraPrep™ reagent and then incubated for 15 min at room temperature with anti-V5-FITC antibody; mock incubation with the antibody served as the control. Whole cell expression of each construct was estimated by flow cytometry. The *symbols* represent means ± S.E. of three independent experiments; *, $p < 0.001$ *versus* control.

comparable with that for wild-type RAMP2 (Fig. 5). Moreover, immunocytochemical analysis showed that almost all of both mutants remained in the ER, representing a pool of newly synthesized molecules not yet transported to the cell surface (Fig. 6). Although they were transfected into CRLR-GFP-expressing cells, however, Δ166- and Δ167-RAMP2 largely failed to transport CRLR-GFP to the cell surface, resulting in significant reductions in specific ^{125}I-AM binding and AM-evoked cAMP production (Table 1). This suggests that the 168th and 169th amino acids (SK sequence) of RAMP2 are important for cell surface delivery of CRLR. The reason for the discrepancy between the IC_{50} and EC_{50} remains unclear, however. By contrast, Δ168- and Δ169-RAMP mediated substantially greater levels of cell surface CRLR-GFP expression, so that AM binding and signaling were equivalent to that seen with wild-type RAMP2 (Table 1). All of the RAMP3 truncation mutants appeared together with CRLR-GFP at the cell surface (Fig. 6*A*), and the resultant receptors showed AM binding and signaling that was comparable with that seen with wild-type RAMP3 (Table 1).

Among the RAMP2 mutants, Δ166 significantly reduced internalization of CRLR-GFP (Fig. 7). Conversely, the Δ139- and Δ140-RAMP3 mutants mediated significantly greater CRLR-GFP internalization than wild-type RAMP3 (Fig. 7). Such increases were not seen with Δ141-RAMP3, and CRLR-GFP internalization mediated by Δ142, Δ143, and Δ144 was equal to that seen with wild-type RAMP3. Thus, the presence of amino acids 141 and 142 (SK sequence) of RAMP3 leads to significant decreases in CRLR internalization.

Characteristics of hRAMP C-tail Chimeras—The SK sequence is highly conserved in the C-tails of all three hRAMPs (Fig. 1) as well as in RAMP isoforms from other species (17). We therefore tested whether exchanging C-tails would affect the cellular trafficking of CRLR-GFP. Given that hRAMP2 promoted CRLR internalization more effectively than other hRAMP isoforms did and that there were no differences in CRLR surface delivery and internalization by hRAMP1 and -3, we constructed four RAMP chimeras (RAMP1/2, -2/1, -2/3, and -3/2) by taking advantage of unique restriction sites that enabled us to generate four hybrid genes. These RAMP chimeras were then transiently transfected into HEK293 cells stably expressing CRLR-GFP and characterized by FACS analysis. As shown in Table 2, cell surface expression and evoked CRLR-GFP internalization of all four chimeras was comparable with

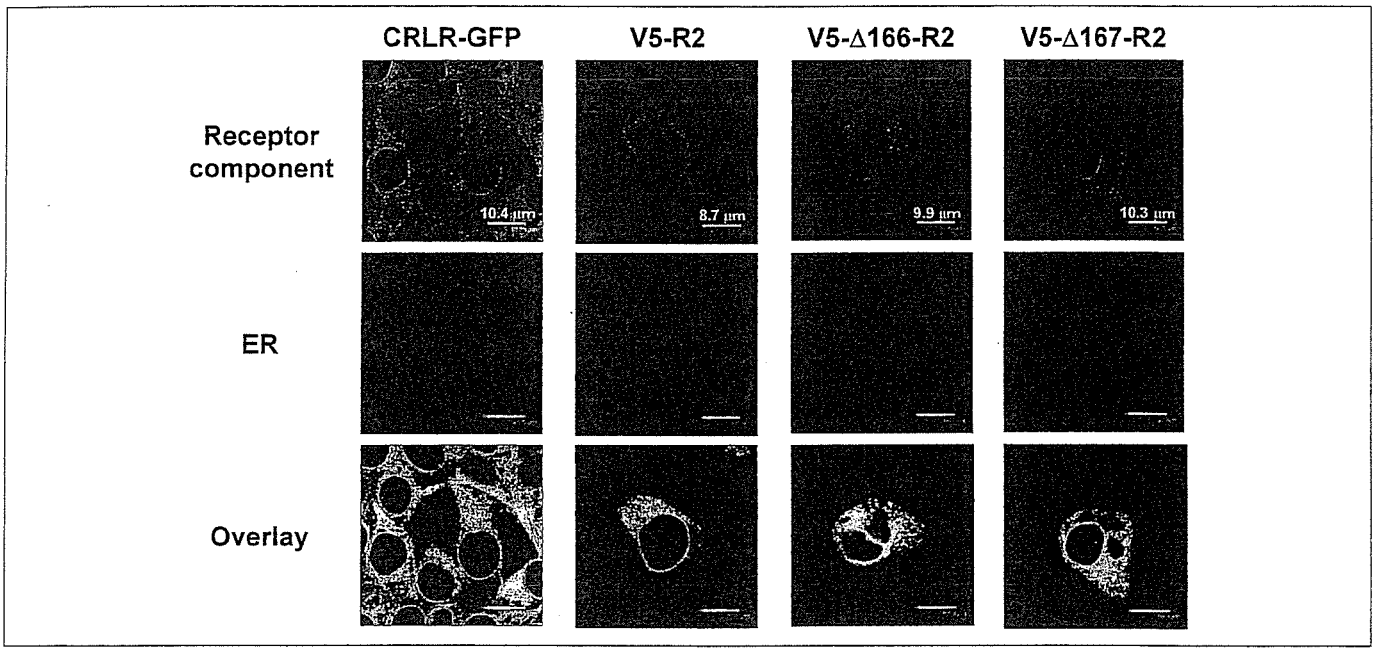

FIGURE 6. **Intracellular localization of V5-hRAMP2 and its truncation mutants.** The indicated RAMP2 constructs were transiently transfected into HEK-293 cells, after which their subcellular distribution was assessed by confocal microscopy in permeabilized cells using anti-V5-FITC antibody. Calnexin (for the ER) was visualized using the appropriate secondary antibody (Alexa Fluor® 594). Co-localization with the ER marker was determined by overlay of the images (*lower panels*). HEK-293 cells stably expressing CRLR-GFP served as the control for co-localization of CRLR-GFP and the ER (*left panels*). *Bar*, ~10 μm.

TABLE 1

Characterization of HEK-293 cells expressing CRLR-GFP and progressive V5-RAMP2 and -3 truncation mutants

The indicated RAMP constructs were transiently transfected into CRLR-GFP-expressing HEK-293 cells. Surface expression of each construct was estimated by flow cytometry. The results represent the means ± S.E. of three independent experiments.

	Cell surface expression (% V5-RAMP2 or -3)	^{125}I-AM binding		AM-evoked cAMP production	
		IC_{50}	Specific binding (% V5-RAMP2 or -3)	EC_{50}	Maximal responses (% V5-RAMP2 or -3)
	%	nM	%	nM	%
V5-RAMP2 (R2)	100	12.2 ± 5.0	100	0.38 ± 0.14	100
V5-Δ166-R2	14.6 ± 1.5[a]	>1000	31.8 ± 1.4[a]	0.16 ± 0.07	37.9 ± 4.7[a]
V5-Δ167-R2	29.0 ± 2.3[a]	>1000	48.0 ± 2.9[a]	0.21 ± 0.09	52.3 ± 1.8[a]
V5-Δ168-R2	61.7 ± 5.5	13.7 ± 5.3	98.4 ± 7.2	0.26 ± 0.22	73.8 ± 20.5
V5-Δ169-R2	83.6 ± 7.8	12.9 ± 3.5	95.8 ± 3.9	0.10 ± 0.06	87.8 ± 19.3
V5-Δ172-R2	55.9 ± 8.1	18.0 ± 6.0	83.1 ± 2.4[a]	0.24 ± 0.04	61.5 ± 4.9
V5-RAMP3 (R3)	100	560 ± 100	100	0.41 ± 0.25	100
V5-Δ139-R3	89.3 ± 6.0	257 ± 49	107 ± 4.3	0.20 ± 0.08	93.8 ± 12.1
V5-Δ140-R3	79.7 ± 5.3	687 ± 70	93.9 ± 1.7	2.50 ± 1.49	91.0 ± 5.7
V5-Δ141-R3	89.1 ± 11.6	317 ± 73	114 ± 1.3[a]	0.30 ± 0.14	116 ± 7.5
V5-Δ142-R3	79.4 ± 9.7	483 ± 193	114 ± 4.5	0.98 ± 0.31	101 ± 8.6
V5-Δ143-R3	84.0 ± 12.8	386 ± 307	111 ± 11.4	0.38 ± 0.21	113 ± 21.6
V5-Δ144-R3	78.2 ± 10.3	383 ± 105	114 ± 6.1	0.13 ± 0.09	102 ± 12.1

[a] $p < 0.03$ *versus* corresponding control (V5-RAMP2 or -3).

that seen with the respective wild-type RAMPs. Thus, exchanging C-tails did not affect RAMP-mediated surface delivery or internalization of CRLR.

Effect of hRAMP C-tail Deletion on Receptor Recycling—For recycling studies, cells were pretreated with 10 μg/ml cycloheximide and 10 μg/ml brefeldin A to respectively inhibit *de novo* protein synthesis and cause disassembly of the Golgi apparatus (29); neither of these reagents had any effect of their own on CGRP- or AM-induced internalization of CRLR-GFP/RAMPs (data not shown). Subsequent treatment of cells with 1 μM αCGRP or AM for 60 min elicited a loss of cell surface receptors that persisted for at least 2 h after washing out the ligands (Fig. 8*A*). Very similar results were seen with Δ139-RAMP1, Δ166-RAMP2, and Δ139-RAMP3, suggesting the RAMP C-tails are not involved in lysosomal sorting of CRLR or the binding of protein(s) that determine the fate of internalized receptors.

Internalization and Recycling of AM_2 Receptors in Cells Cotransfected with hNSF—It was recently shown that, unlike NHERF, NSF contains no recognizable PDZ domains (30) but nonetheless interacts with the PDZ motif of hRAMP3, enabling internalized AM_2 receptors to undergo slow recycling (18). Conversely, NSF enhances β-arrestin 1-mediated β_2-AR internalization (31). Notably, although rat and mouse RAMP3 C-tails contain a RLL sequence instead of a PDZ motif, NSF also promotes recycling of these CRLR/RAMP3 heterodimers (18). With the aim of better understanding the role of NSF in AM_2 receptor trafficking, in the present study, we tested whether the reported effects of hNSF on CRLR/RAMP3 trafficking are reproduced in HEK-293 cells endogenously expressing hNSF and in hNSF transfectants.

We first confirmed that NSF was indeed endogenously expressed in HEK-293 cells by identifying both NSF mRNA and protein in the

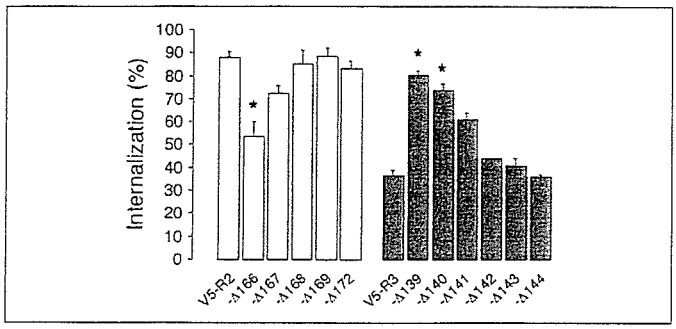

FIGURE 7. **FACS analysis of internalization of hCRLR with progressive hRAMP2 and -3 truncation mutants.** The indicated RAMP constructs were transiently transfected into CRLR-GFP-expressing HEK-293 cells. Surface expression of each construct was estimated by flow cytometry before and after exposing cells to 1 μM AM for 60 min. The results represent the means ± S.E. of three independent experiments; *, $p < 0.003$ *versus* corresponding control (V5-RAMP2 or -3).

TABLE 2

FACS analysis of cell surface delivery and internalization of CRLR-GFP and V5-RAMP chimeras in which the C-tails were exchanged among the three RAMPs

The indicated V5-RAMPs or their chimeras were transiently transfected into CRLR-GFP-expressing HEK-293 cells. Surface expression of each construct was estimated by flow cytometry before and after exposing cells to 1 μM αCGRP or AM for 60 min. The results represent the means ± S.E. of three independent experiments.

	Cell surface expression	Internalization
	%	%
V5-RAMP1	51.8 ± 3.7	50.0 ± 4.3
V5-RAMP2	23.2 ± 2.7	94.5 ± 1.6
V5-RAMP3	46.3 ± 4.8	35.5 ± 1.8
V5-RAMP1/2	49.7 ± 5.6	53.7 ± 7.2
V5-RAMP2/1	25.8 ± 2.3	91.8 ± 0.4
V5-RAMP2/3	19.5 ± 1.4	88.2 ± 1.2
V5-RAMP3/2	44.9 ± 6.1	36.7 ± 3.8

cells (Fig. 8, *B* and *C*). Thereafter, we determined that the levels of the transcript were unaffected by transfection of CRLR-GFP alone or together with V5-RAMP3 (Fig. 8*D*). When NSF was transfected into otherwise untransfected HEK-293 cells and into CRLR-GFP transfectants, levels of its transcript were markedly higher than their endogenous levels in both (Fig. 8*B*). In those cases, Western analysis of NSF protein yielded a single, strong 76-kDa band that was identical to the band obtained when endogenous NSF was probed (Fig. 8*C*), which confirmed that our NSF transfection system worked appropriately. Exposure to 10 nM or 1 μM AM for 60 min induced a rapid decline in cell surface CRLR-GFP/V5-RAMP3 that persisted for at least 4 h after washing out the AM (Fig. 8*D*). Cotransfection of NSF had no effect on these internalization kinetics, and recycling of CRLR/RAMP3 heterodimers, if it occurred, was highly inefficient, even in the presence of abundant NSF (Fig. 8*D*).

DISCUSSION

Since their discovery, there have been only a few reports addressing the functions of the respective C-tails of the three RAMP isoforms (17–19, 32, 33); more extensively studied have been their extracellular domains (11–13, 17, 32, 34, 35). Consequently, whereas nearly all highly conserved residues are known to play key roles in the function and trafficking of cell surface receptors, nothing is known about the functions of the highly conserved Ser and Lys resides within RAMP C-tails. In the present study, we showed that deleting the C-tail from RAMP3 (Δ139-RAMP3) significantly enhanced AM-induced CRLR-GFP internalization but did not affect the targeting of CRLR-GFP to the cell surface or AM binding and signaling. It is therefore unlikely that the truncation of RAMP3 promoted AM-induced conformational changes in the heterodimeric receptors that would alter the binding of AM and/or the interaction of the receptor with G proteins. On the other hand, like wild-type RAMP3, all of the tested RAMP3 truncation mutants that contained the SK sequence (Δ142-, Δ143-, and Δ144-RAMP3) mediated CRLR-GFP internalization less efficiently than those that did not (Δ139-, Δ140-, or Δ141-RAMP3). We also found that substituting the RAMP3 C-tail with the RAMP2 C-tail, which also contains a SK sequence, had no effect on the AM-induced CRLR-GFP internalization. Taken together, these results suggest that the SK sequence participates in the negative regulation of CRLR/RAMP3 internalization.

The Ser/Thr residues present in the C-tails of the three RAMP have been thought to be potential phosphorylation sites, but Hilairet *et al.* (6) showed that in HEK-293 cells overexpressing CRLR/RAMP heterodimers, agonists rapidly promote phosphorylation of CRLR but not RAMP. They also demonstrated that internalization of the heterodimeric receptors was dependent on β-arrestins (6). In the present study, complete removal of the respective RAMP C-tails did not diminish the maximal extent of internalization. It therefore seems unlikely that β-arrestins interact with the RAMP C-tails.

Similar in function to the SK sequence, a dileucine (LL) motif, which is conserved among GPCRs (36), is also present in the C-tail of RAMP3. This motif negatively regulates lutropin/choriogonadotropin receptor (LHR) internalization, since leucine-to-alanine mutations increased the agonist-stimulated internalization of the receptor (37). It is thought that the LL motif participates in protein sorting through direct interaction with two clathrin adaptor protein (AP) complexes, AP-1 and AP-2 (38–40), and the point mutations disrupted the interaction of the LHR with AP-2 at the plasma membrane (39). On the other hand, these mutations are believed to enhance the binding of β-arrestins to the LHR, thereby promoting bridge formation between β-arrestins and clathrin (37). We suggest that, instead of β-arrestins, the RAMP3 C-tail may interact with other intracellular proteins similar to LRP6, another GPCR accessory protein that interacts with axin and catinin (41).

We believe it is noteworthy that the hRAMP3 C-tail contains not only a LL sequence but also a type I PDZ binding sequence (see Fig. 1). Recently, NHERF-1 was found to interact with the PDZ motif of hRAMP3, resulting in complete inhibition of CRLR/RAMP3 internalization (33). In that case, NHERF-1 is thought to act by tethering surface AM_2 receptors to the actin cytoskeleton in a manner also seen with epidermal growth factor receptors (42). By contrast, NHERF-1 promotes the agonist-mediated recycling of β_2-ARs, which also have a PDZ motif (SLL) (30). The mechanism by which NHERF-1 exerts these differing effects on different GPCRs remains unknown. In the present study, three RAMP3 truncation mutants (Δ142-, Δ143-, and Δ144-RAMP3) and the RAMP3/2 chimera, all of which lack both the LL and PDZ sequences, failed to enhance the AM-induced CRLR-GFP internalization. However, this does not preclude the possibility that the level of endogenous NHERF-1 expression in HEK-293 cells used was insufficient to modulate the behavior of the overexpressed RAMP3.

We also showed that deleting the C-tail of RAMP2 impaired the targeting of the CRLR-GFP to the cell surface, thereby markedly reducing AM binding and signaling. Most of the newly synthesized Δ166-RAMP2 remained in the ER along with CRLR-GFP. By contrast, removing the C-tail from RAMP1 or -3 did not diminish surface delivery of the respective receptors. All of the RAMP2 mutants containing an SK sequence (Δ168-, Δ169-, and Δ172-RAMP2) showed better surface CRLR-GFP expression than was seen with Δ166-RAMP2, which lacked the SK sequence. Apparently, the SK sequence in the RAMP2 C-tail is involved in the proper membrane localization of the CRLR/RAMP2. To our knowledge, there have

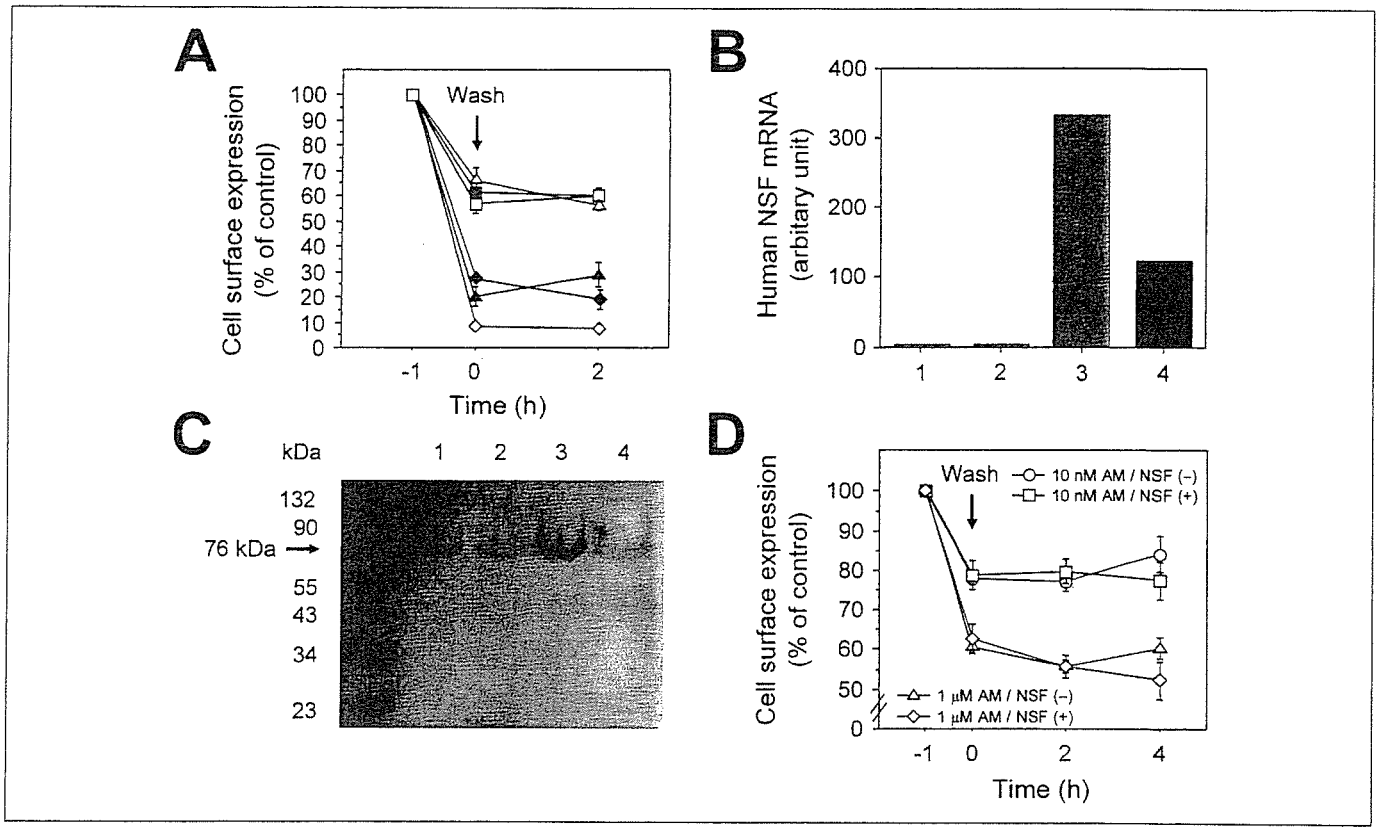

FIGURE 8. **The fates of internalized hCRLR and hRAMPs and their C-terminal deletion mutants.** *A*, FACS analysis of recycling of the internalized heterodimeric receptors. HEK-293 cells stably expressing CRLR-GFP were transiently transfected with each RAMP construct (*symbols* are the same as in Fig. 3*B*), after which they were incubated for 60 min with 1 μM αCGRP or AM plus 10 μg/ml cycloheximide and 10 μg/ml brefeldin A. The cells were then washed with prewarmed PBS and labeled with the indicated antibodies. Cell surface expression of each construct was estimated by flow cytometry. *Bars* represent means ± S.E. of three independent experiments. *B*, endogenous and transiently transfected hNSF mRNA levels. *1*, intact HEK-293 cells; *2*, HEK-293 cells stably expressing CRLR-GFP; *3*, NSF-transfected HEK-293 cells; *4*, NSF-transfected HEK-293 cells stably expressing CRLR-GFP. Expression of NSF mRNA was assessed using real time quantitative PCR with the appropriate primers and probes. Levels of NSF mRNA were normalized to that of GAPDH mRNA, which served as an internal control. *Bars* represent the average of two experiments. *C*, Western analysis of endogenous NSF and overexpressed NSF in HEK-293 cells. Equal aliquots of protein (20 μg) were subjected to 10% SDS gel electrophoresis. *Lane 1*, cells expressing empty vector (*Mock*); *lane 2*, cells stably expressing CRLR-GFP; *lane 3*, cells transiently expressing NSF; *lane 4*, cells expressing both CRLR-GFP and NSF. The blots shown are representative of three independent experiments. *D*, FACS analysis of the recycling of CRLR and RAMP3 in the presence and absence of NSF. CRLR-GFP-expressing cells were transiently transfected with V5-RAMP3 plus empty vector or NSF, after which they were incubated for 60 min with 10 nM or 1 μM AM plus 10 μg/ml cycloheximide and 10 μg/ml brefeldin A. The cells were then treated as described in *A*. Cell surface expression of each construct was estimated by flow cytometry. The *symbols* represent means ± S.E. of three independent experiments.

been no studies on the relation between the SK sequence and surface delivery of other GPCRs, but the LL sequence in the C-tail of the V_2 vasopressin receptor was found to be crucial for ER-to-Golgi transfer of that receptor, presumably by helping establish a correct and transport-competent folding state (36). Similarly, RAMPs appear to mediate transport of the CRLR from the ER to the Golgi, since CRLR was restricted to the ER in the absence of RAMPs (6). It therefore seems likely that the SK sequence in the RAMP2 C-tail, but not that in the RAMP3 C-tail, is essential for the escape of CRLR from the ER. The mechanism underlying the differential effect of the SK sequence on the cellular trafficking of these two AM receptors remains to be determined.

There have been two studies on the effects of CGRP in HEK-293 cells coexpressing hCRLR with a hRAMP1 C-tail deletion mutant (19, 32). One found that the C-tail deletion resulted in a 1-order of magnitude reduction in CGRP-stimulated cAMP formation, but no data on CGRP binding were shown (19). In that case, the 140th residue Gln, but not the SK sequence, most likely determined the affinity of CGRP for the receptor. The other study found no significant changes in CGRP binding or signaling (32). Similarly, we found that deleting the C-tail of RAMP1 had little effect on receptor signaling, as reflected by CGRP-evoked cAMP production, although the binding profile we obtained differed from that obtained in the earlier study (32). This absence of a significant change in the potency of CGRP may indicate that there was little change in the internalization of CRLR-GFP. In contrast to the αCGRP responses, ^{125}I-[Tyr^0]αCGRP binding to CRLR-GFP/Δ139-RAMP1 was much diminished. This discrepancy could be due in part to interference by the extra N-terminal tyrosine residue (Tyr^0). In any event, the contribution of the RAMP1 C-tail to CGRP potency is much smaller than that made by its extracellular domain (13, 17, 32, 34, 35).

Several earlier studies showed that internalized CRLR/RAMP heterodimers are trafficked to lysosomes for degradation (6, 10). It is now recognized that receptor ubiquitination is essential for proper trafficking to lysosomes (43). Indeed, our CRLR-GFP-transfected HEK-293 cells abundantly expressed endogenous ubiquitin, which attaches to lysine residues within the substrate proteins (data not shown). Nevertheless, truncation of RAMP C-tails that removed the Lys residues failed to promote recycling of CRLR-GFP. This raises the possibility that expression of intracellular proteins involved in mediating appropriate receptor recycling was inadequate in the HEK-293 cells used. NSF, like NHERF, is believed to enhance recycling of internalized receptors (44), and it was recently shown that NSF interacts with the PDZ motif of hRAMP3, enabling internalized AM_2 receptors to undergo slow recycling (18). Notably, although rat and mouse RAMP3 tails contain an RLL sequence instead of a PDZ motif, NSF also promoted recycling of CRLR/RAMP3 heterodimers

(18). In the present study, however, the cells abundantly expressed endogenous NSF, making it unlikely that poor expression of NSF underlies the trafficking of CRLR-GFP/RAMP3 to lysosomes without recycling. Even overexpression of NSF in these cells did not alter the AM-mediated trafficking of AM_2 receptors.

The rapid recycling pathway has been best studied and characterized for the β_2-AR, which has a PDZ motif in its C-tail (14, 15, 30) and which requires both NHERF and NSF for its recycling (30, 44). Indeed, among 59 representative seven-transmembrane segment GPCRs tested, NSF bound most strongly to the β_2-AR tail (44). However, a point mutation within the PDZ motif that disrupted the binding of NSF, but not that of NHERF, had no effect on β_2-AR recycling (30). In addition, the β_1-AR and cystic fibrosis transmembrane regulator each contain a C-terminal PDZ binding sequence (SKV and TRL, respectively) and undergo rapid recycling, despite their failure to bind NSF (30). Thus, NSF binding to GPCRs and RAMP3 is not required for recycling of proteins containing PDZ binding sequences.

In summary, our results indicate that the C-tails of hRAMP2 and -3 are involved in hCRLR surface delivery and internalization, respectively, and that the highly conserved SK sequence within their C-tails is a key determinant of the cellular behavior of the AM_1 and AM_2 receptors.

REFERENCES

1. Kitamura, K., Kangawa, K., Kawamoto, M., Ichiki, Y., Nakamura, S., Matsuo, H., and Eto, T. (1993) *Biochem. Biophys. Res. Commun.* **192,** 553–560
2. Eto, T. (2001) *Peptides* **22,** 1693–1711
3. Poyner, D. R., Sexton, P. M., Marshall, I., Smith, D. M., Quirion, R., Born. W., Muff, R., Fischer, J. A., and Foord, S. M. (2002) *Pharmacol. Rev.* **54,** 233–246
4. McLatchie, L. M., Fraser, N. J., Main, M. J., Wise, A., Brown, J., Thompson, N., Solari, R., Lee, M. G., and Foord, S. M. (1998) *Nature* **393,** 333–339
5. Sexton, P. M., Albiston, A., Morfis, M., and Tilakaratne, N. (2001) *Cell Signal.* **13,** 73–83
6. Hilairet, S., Belanger, C., Bertrand, J., Laperriere, A., Foord, S. M., and Bouvier, M. (2001) *J. Biol. Chem.* **276,** 42182–42190
7. Kuwasako, K., Cao, Y-N., Nagoshi, Y., Kitamura, K., and Eto, T. (2004) *Peptides* **25,** 2003–2012
8. Nagoshi, Y., Kuwasako, K., Ito, K., Uemura, T., Kato, J., Kitamura, K., and Eto, T. (2002) *Eur. J. Pharmacol.* **450,** 237–243
9. Muff, R., Born, W., and Fischer, J. A. (2003) *Hypertens. Res.* **26,** 3–8
10. Kuwasako, K., Shimekake, Y., Masuda, M., Nakahara, K., Yoshida, T., Kitaura, M., Kitamura, K., Eto, T., and Sakata, T. (2000) *J. Biol. Chem.* **275,** 29602–29609
11. Kuwasako, K., Kitamura, K., Ito, K., Uemura, T., Yanagita, Y., Kato, J., Sakata, T., and Eto, T. (2001) *J. Biol. Chem.* **276,** 49459–49465
12. Kuwasako, K., Kitamura, K., Onitsuka, H., Uemura, T., Nagoshi, Y., Kato, J., and Eto, T. (2002) *FEBS Lett.* **519,** 113–116
13. Kuwasako, K., Kitamura, K., Nagoshi, Y., Cao Y-N., and Eto, T. (2003) *J. Biol. Chem.* **278,** 22623–22630
14. Koenig, J. A., and Edwardson, J. M. (1997) *Trends. Pharmacol. Sci.* **18,** 276–287
15. Krupnick, J. G., and Benovic, J. L. (1998) *Annu. Rev. Pharmacol. Toxicol.* **38,** 289–319
16. Ferguson, S. S. G. (2001) *Pharmacol. Rev.* **53,** 1–24
17. Hay, D. L., Poyner, D. R., and Sexton, P. M. (2006) *Pharmacol. Ther.* **109,** 173–197
18. Bomberger, J. M., Parameswaran, N., Hall, C. S., Aiyar, N., and Spielman, W. S. (2005) *J. Biol. Chem.* **280,** 9297–9307
19. Steiner, S., Muff, R., Gujer, R., Fischer, J. A., and Born, W. (2002) *Biochemistry* **41,** 11398–11404
20. Hicke, L., and Riezman, H. (1996) *Cell* **84,** 277–287
21. Roth, A. F., and Davis, N. G. (1996) *J. Cell Biol.* **134,** 661–674
22. Martin, N. P., Lefkowitz, R. J., and Shenoy, S. K. (2003) *J. Biol. Chem.* **278,** 45954–45959
23. Shenoy, S. K., and Lefkowitz, R. J. (2003) *J. Biol. Chem.* **278,** 14498–14506
24. Kuwasako, K., Cao, Y-N., Nagoshi, Y., Tsuruda, T., Kitamura, K., and Eto, T. (2004) *Mol. Pharmacol.* **65,** 207–213
25. Aiyar, N., Rand, K., Elshourbagy, N. A., Zeng, Z., Adamou, J. E., Bergsma, D. J., and Li, Y. (1996) *J. Biol. Chem.* **271,** 11325–11329
26. Guon, X.-M., Kobilka, T. S., and Kobilka, B. K. (1992) *J. Biol. Chem.* **267,** 21995–21998
27. Nagoshi, Y., Kuwasako, K., Cao, Y-N., Kitamura, K., and Eto, T. (2004) *Biochem. Biophys. Res. Commun.* **314,** 1057–1063
28. Cao, Y-N., Kuwasako, K., Kato, J., Yanagita, T., Tsuruda, T., Kawano, J., Nagoshi, Y., Chen, A. F., Wada, A., Suganuma, T., Eto, T., and Kitamura, K. (2005) *Biochem. Biophys. Res. Commun.* **332,** 866–872
29. Xu, J., and Tse, F. W. (1999) *J. Biol. Chem.* **274,** 19095–19102
30. Gage, R. M., Matveeva, E. A., Whiteheart, S. W., von Zastrow, M. (2005) *J. Biol. Chem.* **280,** 3305–3313
31. McDonald, P. H., Cote, N. L., Lin, F-T., Premont, R. T., Pitcher, J. A., and Lefkowitz, R. J. (1999) *J. Biol. Chem.* **274,** 10677–10680
32. Fitzsimmons, T. J., Zhao, X., and Wank, S. A. (2003) *J. Biol. Chem.* **278,** 14313–14320
33. Bomberger, J. M., Spielman, W. S., Hall, C. S., Weinman, E. J., and Parameswaran, N. (2005) *J. Biol. Chem.* **280,** 23926–23935
34. Fraser, N. J., Wise, A., Brown, J., McLatchie, L. M., Main, M. J., and Foord, S. M. (1999) *Mol. Pharmacol.* **55,** 1054–1059
35. Hilairet, S., Foord, S. M., Marshall, F. H., and Bouvier, M. (2001) *J. Biol. Chem.* **276,** 29575–29581
36. Schulein, R., Hermosilla, R., Oksche, A., Dehe, M., Wiesner, B., Krause, G., and Rosenthal, W. (1998) *Mol. Pharmacol.* **54,** 525–535
37. Nakamura, K., and Ascoli, M. (1999) *Mol. Pharmacol.* **56,** 728–736
38. Dietrich, J., Kastrup, J., Nielsen, B. L., Odum, N., and Geisler, C. (1997) *J. Cell Biol.* **138,** 271–281
39. Kirchhausen, T., Bonifacino, J. S., and Riezman, H. (1997) *Curr. Opin. Cell Biol.* **9,** 488–495
40. Rapoport, I., Chen, Y-C., Cupers, P., Shoelson, S. E., and Kirchhausen, T. (1998) *EMBO J.* **17,** 2148–2155
41. Tamai, K., Semenov, M., Kato, Y., Spokony, R., Liu, C., Katsuyama, Y., Hess, F., Saint-Jeannet, J. P., and He, X. (2000) *Nature* **407,** 530–535
42. Lazar, C. S., Cresson, C. M., Lauffenburger, D. A., and Gill, G. N. (2004) *Mol. Biol. Cell* **15,** 5470–5480
43. Wojcikiewicz, R. J. H. (2004) *Trends Pharmacol. Sci.* **25,** 35–41
44. Heydorn, A., Sondergaard, B. P., Ersboll, B., Holst, B., Nielsen, F. C., Haft, C. R., Whistler, J., and Schwartz, T. W. (2004) *J. Biol. Chem.* **279,** 54291–54303

Available online at www.sciencedirect.com
ScienceDirect
Journal of Molecular and Cellular Cardiology 42 (2007) 88–97
Journal of Molecular and Cellular Cardiology
www.elsevier.com/locate/yjmcc

Original article

Transplantation of mesenchymal stem cells attenuates myocardial injury and dysfunction in a rat model of acute myocarditis

Shunsuke Ohnishi [a,*,1], Bobby Yanagawa [a,1], Koichi Tanaka [a], Yoshinori Miyahara [a], Hiroaki Obata [a,b], Masaharu Kataoka [a], Makoto Kodama [b], Hatsue Ishibashi-Ueda [c], Kenji Kangawa [d], Soichiro Kitamura [e], Noritoshi Nagaya [a,*]

[a] *Department of Regenerative Medicine and Tissue Engineering, National Cardiovascular Center Research Institute, Fujishirodai 5-7-1, Osaka 565-8565, Japan*
[b] *Division of Cardiology, Niigata University Graduate School of Medical and Dental Sciences, Niigata, Japan*
[c] *Department of Pathology, National Cardiovascular Center, Osaka, Japan*
[d] *Department of Biochemistry, National Cardiovascular Center Research Institute, Osaka, Japan*
[e] *Department of Cardiovascular Surgery, National Cardiovascular Center, Osaka, Japan*

Received 11 May 2006; received in revised form 29 August 2006; accepted 2 October 2006
Available online 13 November 2006

Abstract

Acute myocarditis is a non-ischemic inflammatory disease of the myocardium for which there is currently no specific treatment. We have previously shown that mesenchymal stem cells (MSC) can ameliorate heart injury during acute ischemia and in dilated cardiomyopathy; however, the therapeutic potential in acute myocarditis is unclear. In this study, we investigated the ability of MSC to attenuate myocardial injury and dysfunction during the acute phase of experimental myocarditis. Ten-week-old male Lewis rats were injected with porcine myosin to induce myocarditis. Cultured MSC (3×10^6 cells/rat) were injected intravenously 7 days after myosin injection. At 3 weeks, myosin injection resulted in severe inflammation and significant deterioration of cardiac function. MSC transplantation attenuated increases in CD68-positive inflammatory cells and monocyte chemoattractant protein-1 (MCP-1) expression in myocardium, and improved cardiac function in this model. Furthermore, myocardial capillary density was higher in myocarditis tissue, and was further increased by MSC transplantation. *In vitro*, cultured adult rat cardiomyocytes were injured in response to MCP-1, whereas this effect was attenuated by MSC-derived conditioned medium, suggesting cardioprotective effects of MSC acting in a paracrine manner. MSC transplantation attenuated myocardial injury and dysfunction in a rat model of acute myocarditis, at least in part through paracrine effects of MSC.

Keywords: Acute myocarditis; Mesenchymal stem cell; Paracrine effect; Cytokine; Cell death

1. Introduction

Acute myocarditis is a non-ischemic heart disease characterized by myocardial inflammation and edema. This disease is associated with rapidly progressive heart failure, arrhythmias and sudden death [1,2]. Although the early evidence for efficacy of immunoglobulin and interferon therapy appears promising, these results have yet to be demonstrated in randomized or controlled clinical trials. The current options are restricted to supportive care for heart failure or arrhythmias. The lack of specific treatment and the potential severity of the illness emphasize the importance of novel and effective therapeutic strategies for myocarditis.

Mesenchymal stem cells (MSC) are multipotent stem cells present in adult tissues, and have the ability to differentiate into a variety of lineages, including vascular smooth muscle cells, endothelial cells and cardiomyocytes [3,4]. We have previously reported that bone marrow-derived MSC engrafted in experimental myocardial infarction expressed both cardiac and endothelial phenotypes in the heart, and further increased capillary density and decreased the infarct size [5]. Moreover, we have recently demonstrated that monolayered MSC derived from adipose tissue reversed wall thinning in the scar area and improved cardiac function in rats with myocardial infarction [6]. The cardioprotective effects of MSC are known to be mediated

* Corresponding authors. Tel.: +81 6 6833 5012; fax: +81 6 6833 9865.
E-mail addresses: sonsihi@ri.ncvc.go.jp (S. Ohnishi), nnagaya@ri.ncvc.go.jp (N. Nagaya).
[1] Drs Ohnishi and Yanagawa contributed equally to this study.

0022-2828/$ - see front matter © 2006 Elsevier Inc. All rights reserved.
doi:10.1016/j.yjmcc.2006.10.003

not only by their differentiation into vascular cells and cardiomyocytes, but also by their ability to supply large amounts of angiogenic, anti-apoptotic and mitogenic factors [5–7]. These findings suggest the therapeutic potential of MSC for heart failure. However, whether intravenously transplanted MSC attenuate myocardial inflammation and cardiac dysfunction in acute myocarditis remains unknown.

In the present study, we used porcine myosin-induced acute myocarditis in Lewis rats. This model closely resembles human giant cell myocarditis, a frequently fatal disorder characterized by multinucleated giant cells in the myocardium [8]. To examine the therapeutic potential of MSC in the acute phase of myocarditis, MSC were intravenously injected into rats 7 days after myosin injection.

Thus, the purposes of this study were 1) to investigate whether intravenous transplantation of MSC improves cardiac function and pathological findings including myocardial inflammation in rats with myosin-induced myocarditis, and 2) to investigate the underlying mechanisms responsible for the effects of MSC.

2. Materials and methods

2.1. Animals

Ten-week-old male Lewis rats (Japan SLC, Hamamatsu, Japan) were used in all experiments, and were maintained in our animal facilities. The experimental protocols were approved by The Animal Care Committee of the National Cardiovascular Center.

2.2. Preparation of cardiac myosin

Purified cardiac myosin from the ventricular muscle of pig hearts was prepared according to a procedure described previously [8]. The antigen was dissolved at a concentration of 20 mg/ml in phosphate-buffered saline (PBS) containing 0.3 M KCl, mixed with an equal volume of complete Freund's adjuvant containing 11 mg/ml *Mycobacterium tuberculosis* (Difco Laboratories, Sparks, MD, USA). Rats were anesthetized with an intraperitoneal injection of 20 mg/kg sodium pentobarbital, and 0.1 ml of the antigen-adjuvant emulsion was injected into the each footpad.

2.3. Acute myocarditis model

Forty-five rats were randomly divided into three groups and received the following treatment: 1) 0.2 ml saline and sham surgery (Sham group, $n=15$), 2) 0.2 ml cardiac myosin antigen and sham surgery (MyoC group, $n=15$), and 3) 0.2 ml cardiac myosin followed by MSC transplantation 7 days post-myosin injection (MyoC+MSC group, $n=15$). Rats were weighed and observed daily for signs of morbidity and for death.

2.4. Preparation and transplantation of bone marrow-derived MSC

MSC were prepared as described previously [5]. Briefly, bone marrow cells were isolated by flushing out the femoral and tibial cavities with PBS, and plated onto 10-cm dishes in complete culture medium: Dulbecco's Modified Eagle's Medium (DMEM), 15% fetal bovine serum, 100 U/ml penicillin and 100 μg/ml streptomycin. Five days after plating, non-adherent cells were removed, and adherent cells were further propagated for 4 to 5 passages.

Seven days after myosin injection, MSC (3×10^6 cells) or vehicle (0.9% saline) was intravenously administered via the jugular vein. Sham rats also received saline administration but without myosin injection.

2.5. Hemodynamic studies

Hemodynamic studies were performed on day 21 post-myosin injection. Anesthesia was maintained with an intraperitoneal injection of 20 mg/kg sodium pentobarbital, and a 1.5 Fr micromanometer-tipped catheter was placed in the left ventricle through the right carotid artery (Millar Instruments, Houston, TX, USA). Heart rate (HR) was also monitored by electrocardiography. HR, mean arterial pressure (MAP), left ventricular systolic pressure (LVSP), left ventricular end-diastolic pressure (LVEDP), maximum dP/dt (Max dP/dt) and minimum dP/dt (Min dP/dt) were used as indices of hemodynamics, and recorded simultaneously during ventilation after a minimum equilibration period of 20 min.

2.6. Echocardiographic studies

Echocardiography was performed on day 21 post-myosin injection. Rats were anesthetized with an intraperitoneal injection of 20 mg/kg sodium pentobarbital. A 12 MHz probe was placed at the left 4th intercostal space for M-mode imaging using 2D echocardiography (Sonos 5500, Philips, Bothell, WA, USA). Left ventricular systolic dimension (LVDs), left ventricular diastolic dimension (LVDd), anterior wall thickness (AWT), posterior wall thickness (PWT) and ejection fraction (EF) were measured, and taken as an average of three beats. Fractional shortening (%FS) was calculated as $(LVDd-LVDs)/LVDd\times100$.

2.7. Histological examination

The heart was excised above the origin of the great vessels, and heart weight and body weight were recorded on day 21 post-myosin injection. Portions of the midventricular heart, spleen, pancreas, kidney and liver were fixed with 4% paraformaldehyde, embedded in paraffin, sectioned at 4-μm thickness, stained with either hematoxylin and eosin (H & E) or Masson's trichrome, and subjected to immunohistochemical staining. H & E-stained sections were evaluated by a cardiovascular pathologist (H.I.-U.) for the characterization of myocardial injury and inflammation without knowledge of the experimental groups, on the following scale: 0, absent or questionable presence; 1, limited focal distribution; 2–3, intermediate severity; and 4, coalescent and extensive foci throughout the entire transversely sectioned ventricular tissue.